NTNU
Norwegian University of
Science and Technology

Formation of a shale barrier using numerical and analytical methods

Øyvind Skomedal

Petroleum Geoscience and Engineering
Submission date: June 2016
Supervisor: Rune Martin Holt, IPT

Norwegian University of Science and Technology
Department of Petroleum Engineering and Applied Geophysics

Preface

First of all, I would like to thank my main supervisor Rune Martin Holt for providing me with problem statement, litterature, advices and interesting conversations through my work on project assignment and Master's thesis.

Co-supervisor Erling Fjær has helped me with problem statements, interpretations as well as being very accommodating when help was needed. He also had the main contribution to the derivation of total strain deformation.

I will also thank co-supervisor Liming Li for PFC code development, advices and interpretations related to this software. Jon Steinar Folstad's master's thesis has also been a valuable aid during simulation in PFC.

SINTEF Petroleum has provided me with office and computer with PFC2D license. I've therefore spent a lot of time there and got the opportunity to meet many nice people.

In the end, I would like to thank Eiliv Skomedal for all discussions and the knowledge he has shared.

Øyvind Skomedal
Trondheim
June, 2016

Summary

The petroleum industry is looking for less expensive solutions regarding Plug & Abandonment. Earlier studies have shown incidents that shale formation around a well sometimes deforms and establishes sufficient seal around casing. This may reduce costs of plugging operations significantly, and it is therefore valuable to learn more about this time dependent deformation phenomenon.

This thesis investigates creep and plastic strain as possible causes for this deformation. Analyses on creep are simulated in PFC (Particle Flow Code). The simulations include calibration of strain from a real shale specimen and simulations of creep around a borehole. The calibrated parameters are then applied for the simulations on creep around a borehole to investigate how this real shale behaves during creep in well-scale. Then, creep threshold stresses in the code are evaluated, and it is discovered huge uncertainties regarding this parameter.

The plastic strain deformation part includes a derivation of an expression of total strain around a borehole using the Mohr-Coulomb criterion with altered plastic parameters. Due to its effective stress dependency, the Mohr-Coulomb criterion is well suited to evaluate plastic strain deformation in a borehole surrounded by a shale subjected to long term drainage. After deriving the expression, parameter analyses show that the unconfined residual strength C_0^* has large impact on a rock's ability to deform around a well.

Sammendrag

Petroleumsnæringen ønsker å finne billigere løsninger for permanent gjennplugging av brønn. Tidligere studier har vist til hendelser der skiferformasjonen rundt en brønn noen ganger deformeres og oppnår tilstrekkelig tetning rundt foringsrøret. Dette kan redusere kostnader ved pluggingsprosesser betydelig, og det er derfor nyttig å lære mer om dette tidsavhengige deformasjonsfenomenet.

Denne avhandlingen undersøker kryp og plastisk tøyning som mulige årsaker til denne deformasjonen. Analyser på kryp er simulert i PFC (Particle Flow Code). Simuleringene inkluderer kalibrering av tøyning fra en ekte skiferprøve samt simuleringer av kryp rundt et borehull. De kalibrerte parametrene blir brukt i simuleringene på kryp rundt et borehull for å undersøke hvordan denne virkelige skiferen opptrer i brønnskala. Deretter evalueres kodens kryp-terskelspenning, og det oppdages store usikkerheter vedrørende denne parameteren.

Delen om plastisk deformasjon omfatter en utledning av et uttrykk for total tøyningsdeformasjon rundt et borehull ved hjelp av Mohr-Coulomb-kriteriet med endrede plastiske parametere. På grunn av at det er effektivitetsavhengig, er Mohr-Coulomb-kriteriet godt egnet for å evaluere plastisk deformasjon i et borehull omgitt av en skifer som har vært drenert over lang tid. Etter utledningen av uttrykket, viser parameteranalyser at enaksiell reststyrke C_0^* har stor innvirkning på en steins evne til å deformere rundt en brønn.

Contents

Abbreviations

NORSOK Norsk sokkels konkurranseposisjon

PFC2D Particle flow code 2D

UCS Uniaxial compressive strength

AFS Axial failure strength

QFP Quartz, feldspar and pyrite

TVD True vertical depth

Nomenclature

β	$\frac{\pi}{4} + \frac{\phi}{2}$.
ϵ	Total strain.
$\epsilon_1(t)$	Strain in transient stage as a function of time in creep.
$\epsilon_3(t)$	Strain in tertiary stage as a function of time in creep.
ϵ_θ^p	Tangential plastic strain.
ϵ_e	Elastic strain.
ϵ_p	Plastic strain.
ϵ_r^p	Radial plastic strain.
ϵ_{tot}	Total strain.
λ	Lame's parameter.
μ^*	Friction coefficient.
ϕ	Internal friction angle.

σ_θ	Total tangential stress.
σ'_θ	Effective tangential stress.
σ_h	Total horizontal far field stress.
σ_r	Total radial stress.
σ'_r	Effective radial stress.
$\sigma_r^{elastic}$	Radial stress right at the beginning of elastic region.
$\sigma_r^{plastic}$	Radial stress at the edge of plastic region.
σ_z	Vertical stress on core specimen.
σ'_z	Effective vertical stress.
σ_{conf}	Confining stress on core specimen.
τ	Initial shear stress between elements in PFC.
τ'	Reduced shear stress between elements in PFC.
τ_0	Creep shear stress threshold in PFC.
τ_m	Constant.
C_0	Uniaxial compressive strength.
C_0^*	Unconfined residual strength.
C_1	Integration constant.
C_2	Integration constant.
C'_2	Constant.
$d\lambda_p$	Plastic strain deformation.
G	Lame's parameter.
H	Uniaxial compaction modulus.
k	Friction constant.

k^*	Altered friction constant.
M	Moduli.
n	Constant.
n^*	Slope of confining stress vs axial failure stress.
P_f	Pore pressure.
P_w	Well pressure.
P_{diff}	Differential stress between axial load and confining stress on core specimen.
Q	Free energy activation.
R	Initial well radius.
r	Radial distance from the borehole centre.
R_g	Gas constant.
R_p	Radius of plastic region around a borehole.
R_{def}	New radius as a result of deformation.
T	Temperature.
u	Total radial displacement [m].
$u_{elastic}$	Radial elastic strain displacement.
$u_{plastic}$	Radial plastic strain displacement.
V_0	Creep rate.
Vt	Strain in steady state region in creep.

List of Figures

1 Introduction

Previous studies on shale as a barrier have shown that the rock may form a sufficient seal regarding Plug & Abandonment. Results from (Williams et al, 2009) [1] indicate that the shale has deformed and established sufficient contact between formation and casing and meets up to standard NORSOK requirements on P&A. In addition, studies on borehole cement permeability (McDaniel, 1980) [2] and shale permeability (Torsæter et al, 2014) [3] show that shale has a significant lower permeability than cement. This means that less fluid is capable to leak through the plugged section. Shale is also often located as a cap rock over petroleum reservoirs. This makes the rock type applicable, as these spots are convenient places to plug wells while still allowing side tracking from shallower sections in the future. Applying shale as a barrier can be a more efficient way to plug a well compared to the conventional P&A procedures, as it does not need to perforate or mill sections to establish sufficient sealing with formation. There can be different reasons to the mechanism behind this deformation around borehole. (Williams et al, 2009) [1] suggests creep and shear failure as the most reasonable explanations.

This thesis will conduct numerical simulations and analytical investigations on how shale may deform and generate a barrier around a well. The creep simulations will be conducted in PFC2D (Particle Flow Code 2D), which by (Folstad, 2015) [4] and (Skomedal, 2015) [5] has proven to be a decent tool in order to simulate this phenomenon. The creep model in the software is also based on these previous works, and as for (Folstad, 2015) [4], the simulations will include mimicking strain rate of a real rock before applying this mimicked rock to creep simulation around a well. There will then be investigated what impact the creep threshold τ_0 has on the creep results in the simulation. τ_0 is an important parameter as it decides the creep inducement in the simulations.

The analytical part will derive an expression on total strain deformation around a borehole based on Mohr-Coulomb failure criterion when including altered plastic parameters. There will then be conducted sensitivity analyses which will distinguish important parameters to the aspect of plastic and elastic deformation. In the end, failure analyses by Mohr-Coulomb will investigate stress distributions around a borehole with and without altered plastic parameters.

2 General theory on the creep model

Creep is often referred to as a time dependent deformation which will continue under constant stress. The deformation rate increases as the applied stress increases (Fjær et al, 2014) [6], and it is likely to divide the deformation into three regimes depicted in figure 2.1.

At $t = 0$, the rock has gone through an elastic deformation. As the time moves on with constant stress, the deformation increases with a decreasing rate. This state is referred to the *transient* stage, and if the stress applied here suddenly decreases to zero, the strain at this stage also moves back to zero. The next stage is called *steady state*. Under constant stress, the rock will creep with unchanged strain rate. Some of the elastic strain transfers over to plastic strain, a process referred to as relaxation. This leaves a residual, permanent deformation. As the time goes by, the rock might move over to a region where the strain rate increases. This is referred to *tertiary* stage or accelerating stage and leads quickly to failure.

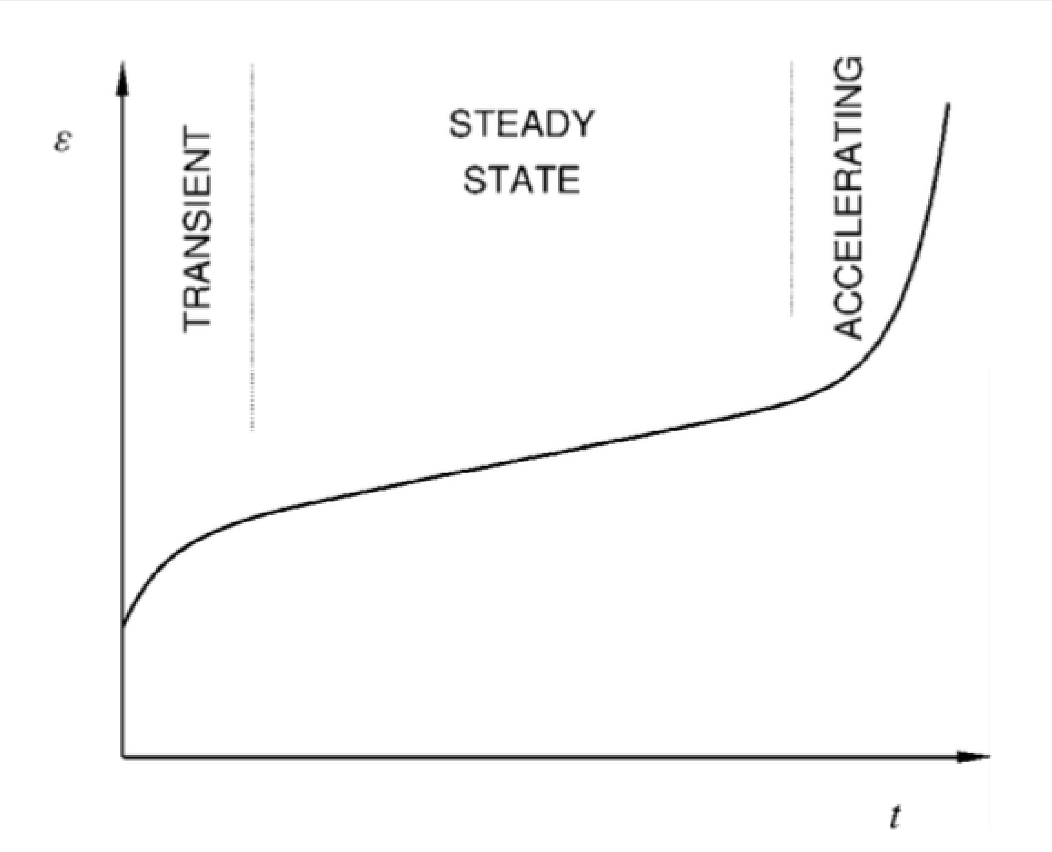

Figure 2.1: (Fjær et al, Ch. 1, 2008) [7] The different stages in creep.

Eq. (2.1) (Jaeger et al, Ch. 9, 2007) [8]) describes the curve in figure 2.1.

$$\epsilon = \epsilon_e + \epsilon_1(t) + Vt + \epsilon_3(t) \tag{2.1}$$

Where ϵ_e represents the initial elastic strain at $t = 0$, $\epsilon_1(t)$ describes the strain at *transient* stage, Vt is the strain in *steady state* region while $\epsilon_3(t)$ is referred to strain in *tertiary* stage. In this thesis the *steady state* region will be investigated. This is because the region describes how stable creep around a borehole behaves. It also correlates to results on previous studies reagerding creep. (Sone and Zoback, 2014) [9], (Bauer et al, 2014) [10], (Zhang et al, 2006) [11], (Kuhn and Mitchell, 1993) [12].

2.1 Description of the numerical creep mechanism

As mentioned in the introduction, PFC is a suitable tool to simulate rock deformation. With this code, a rock can be mimicked if there are sufficient bonding, such as tension and rotation resistance between elements. Note that if enough bonds are broken, failure will occur (Fjær et al, 2016) [13], (Folstad, 2015) [4].

In the simulation in this thesis, all elements are initially bonded and all interactions between elements are directly related to the displacement between elements. Creep is induced by implementing a time dependent plastic part in the bonds between elements. The displacement between elements are now decomposed in both plastic and elastic parts. If the displacement between two elements maintains constant, the creep implementation increases the plastic part, while the elastic part of the decomposition and the associated stresses decreases. This is related to the term relaxation.

A rock will creep if the shear stress between elements exceed the creep threshold τ_0. The shear stress in the bonds between all the elements are denoted as τ. By allowing stress relaxation and no displacement, τ becomes τ' after a time period Δt. If τ' reduces to less than τ_0, creep will cease (eq. (2.2) and figure 2.2).

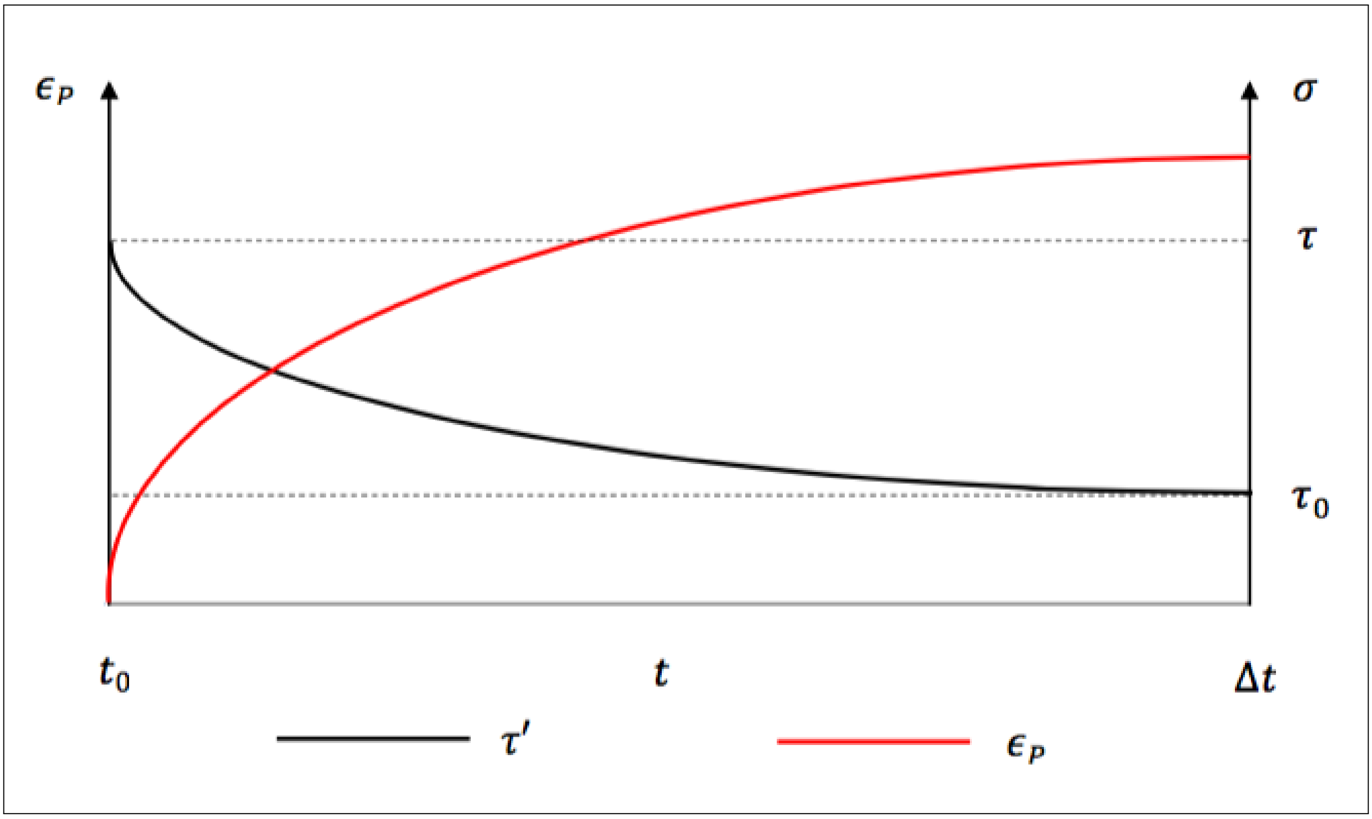

Figure 2.2: Graphical interpretation of relaxation where plastic strain ϵ_p and reduced stress τ' are functions of time t.

Figure 2.2 describes the development on plastic strain and stresses between elements as a function of time. The plastic deformation ceases when the reduced shear stresses τ' approach the creep threshold τ_0. Creep will occur when following:

$$\tau > \tau' > \tau_0 \tag{2.2}$$

The ratio of stresses after and before relaxation is:

$$\alpha = \frac{\tau'}{\tau} \tag{2.3}$$

The stress when there is only elastic strain is written as:

$$\tau = M\Delta\epsilon_e \tag{2.4}$$

Where M is a moduli.

Further, the creep mechanism is induced and the deformation between the elements, which is constant, is decomposed to both elastic and plastic strain as a function of time. Figure 2.3 denotes this decomposition and the corresponding reduced stresses τ' with a red bar bond.

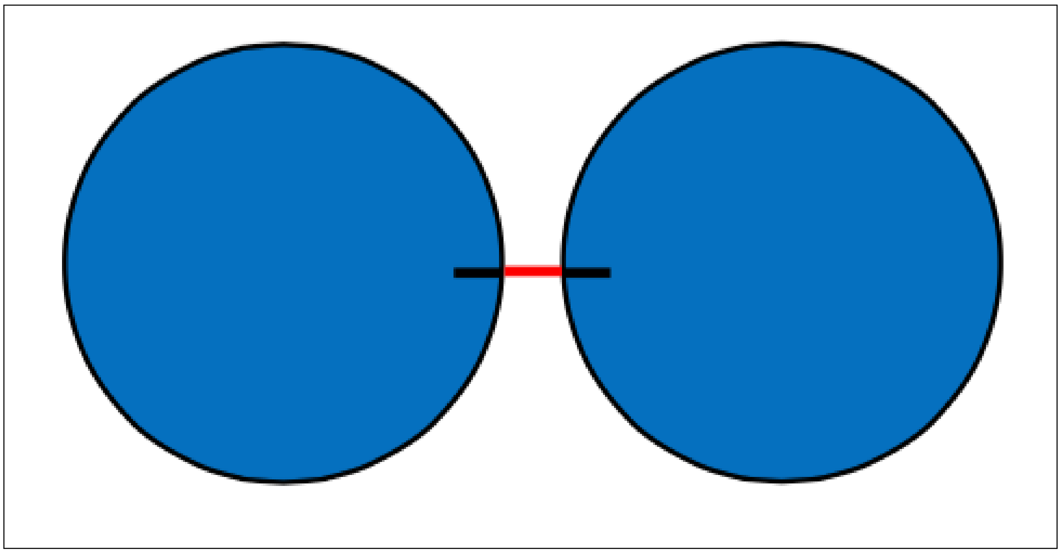

Figure 2.3: Two elements bonded together with stresses τ'. The red bar bond denotes the partially induced plastic strain as well as stresses τ'.

The stresses after relaxation is:

$$\tau' = M\Delta\epsilon_{tot} \tag{2.5}$$

Hence:

$$\alpha = \frac{\tau'}{\tau} = \frac{M\Delta\epsilon_e}{M\Delta\epsilon_{tot}} \tag{2.6}$$

The total displacement term:

$$\Delta\epsilon_e = \Delta\epsilon_{tot} - \Delta\epsilon_p \tag{2.7}$$

Which yields:

$$\alpha = \frac{\tau'}{\tau} = 1 - \frac{M\Delta\epsilon_p}{M\Delta\epsilon_{tot}} \tag{2.8}$$

Combining eq. (2.7) with eq. (2.4) gives:

$$\alpha = \frac{\tau'}{\tau} = 1 - \frac{M\Delta\epsilon_p}{\tau} \tag{2.9}$$

The following equation describes the creep strain through Δt (Jaeger et al,Ch. 9, 2007) [8]:

$$\Delta\epsilon_p = V_0 e^{-Q/R_gT}\left(\frac{\tau}{\tau_m}\right)^n \Delta t \tag{2.10}$$

Where V_0 is related to the strain rate, Q is the free energy activation, T is the absolute temperature, R_g is the gas constant and τ_m and n are constants. This is a general way to explain the creep strain through the period Δt in a micro scale. It can therefore be adapted into PFC since the code relates to bondings in grain dimension.

Inserting eq. (2.10) into eq. (2.9) yields:

$$\alpha = 1 - \frac{MV_0 e^{-Q/R_gT}}{\tau_m^n}\tau^{n-1}\Delta t \tag{2.11}$$

Eq. (2.11) explains how to determine the contact force reduction after the time period Δt due to the stress relaxation. Note that the equation only applies when the reduced contact stresses τ' are greater than the creep threshold

τ_0 (figure 2.2 and eq. 2.2).

3 Simulations

The simulations in this thesis will involve creep around a borehole and calibration. The calibration part is a 2D simulation biaxial test which will, by changing different parameters, mimic a real shale core specimen by matching creep strain rate. The shale will be based on Haynesville (Sone and Zoback, 2014) [9], which is a rather stiff type of rock. A 2D well-scaled simulation will then use these parameters to investigate stress distribution around a borehole during creep. The threshold stresses will be evaluated in both calibration test and well-scale simulation.

3.1 Biaxial calibration test

The biaxial test calibrates the numerical 2D specimen in order to mimic the real specimen from a stiff shale called Haynesville (Sone and Zoback, 2014) [9]. The next section is going to describe the triaxial test conducted on the real specimen, Haynesville.

3.1.1 Creep strain rate on a real specimen

(Sone and Zoback, 2014) [9] conducted several tests on different shale specimens. This thesis will focus on mimicking Haynesville 1. Figure 3.1 shows the mineral composition of the shale determined by powder XDC analysis. It tells that it contains approximately 35 % quartz, feldspar, and pyrite (QFP), 45 % clay+kerogen and 20 % carbonates. The cylindrical sample had a 1" diameter and a length on 2,1" perpendicular to the bedding plane.

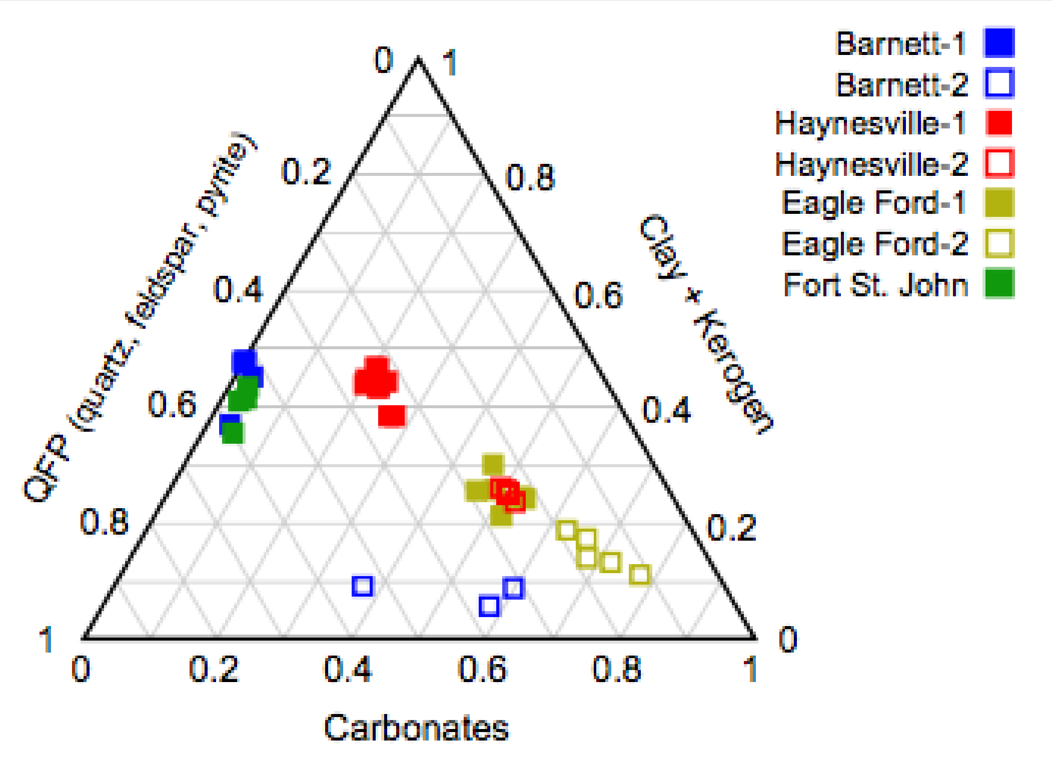

Figure 3.1: (Sone and Zoback, 2014) [9] Ternary plot of the mineral compositions of the different specimens tested.

The triaxial test of Haynesville 1 was conducted with differential pressure P_{diff} increasing step-wise in the vertical direction where each step lasted for 60 seconds. This thesis will focus on the first step on vertical strain on a the Haynesville with a differential stress on $P_{diff} = 32$ MPa. The experiment was conducted in room-temperature, and drained pore pressure in order to avoid poroelastic effects. The strain results are presented in figure 3.2

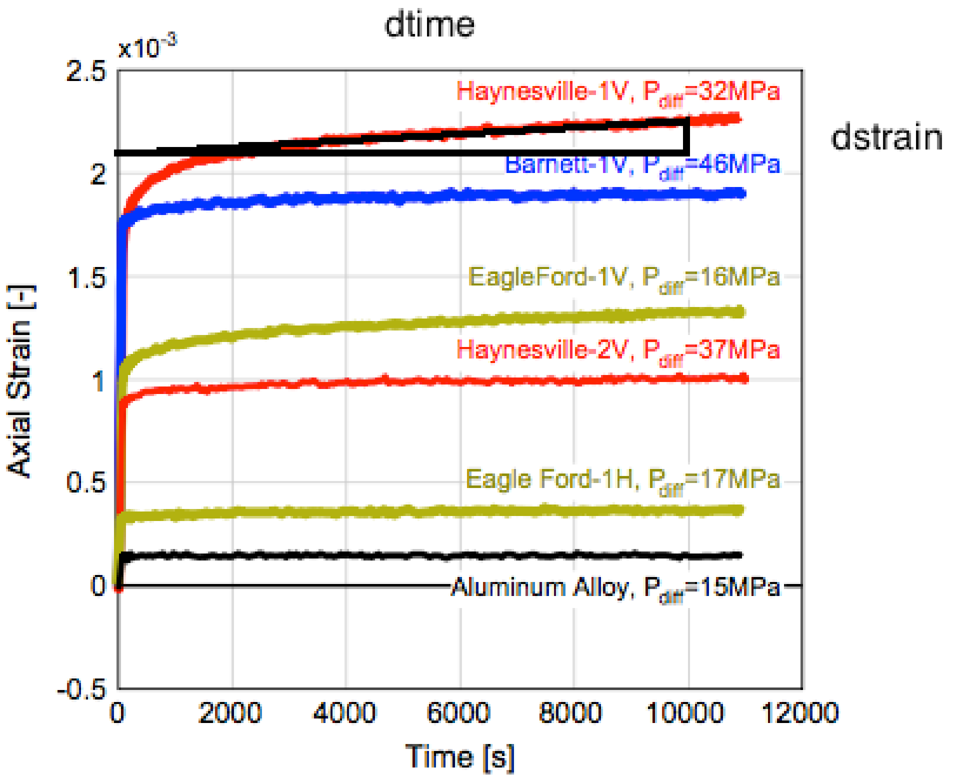

Figure 3.2: (Sone and Zoback, 2014) [9] Strain vs time. The aluminium alloy is shown as a reference for pure elastic behaviour. H and V stand for vertical and horizontal orientation to the bedding plane.

The specimens are exposed for increasing different stresses denoted as P_{Diff} the first 60 seconds, and the rocks show an elastic strain behaviour. The strain rate becomes constant as time moves on. This indicates that the rock has reached the *steady state* stage for creep. The creep strain rate for Haynesville-1V can then be calculated schematically:

$$strainRate = \frac{\Delta\epsilon}{\Delta t} = \frac{\epsilon_2 - \epsilon_1}{t_1 - t_0} = \frac{1,5 * 10^{-4}}{1 * 10^{4}} = 1,5 * 10^{-8}\ s^{-1} \tag{3.1}$$

The next section is going to discuss how to achieve this strain rate for a numerical specimen in PFC.

3.1.2 Creep strain rate from numerical simulation

The calibration is conducted with simulated 2D core specimen which is supposed to mimic a cross section of a real core specimen. Different parameters such as porosity and density are set according to real values. The procedure is based on (Folstad, 2015) [4], who conducted similar work.

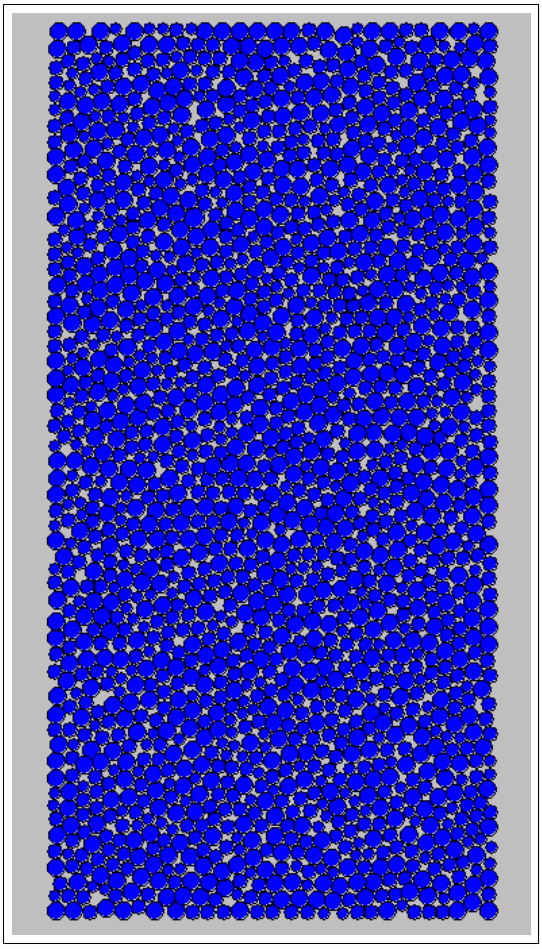

Figure 3.3: 2D ball plot of the initial core specimen.

Figure 3.3 presents the 2D balls bonded together in a cluster shaped as a real core specimen. All walls have an initial applied stress on 30 MPa and bond strength is induced. Then, differential vertical wall stress P_{diff} is applied incrementally and the numerical core specimen undergoes an elastic deformation. When the differential stress P_{diff} has reached 32 MPa, the creep mechanism is induced. The resulting strain rate from the creep mechanism is then recorded and the parameters are presented in figure 3.4. Figure 3.5 presents a flow chart of the calibration method used in order to achieve the desired strain rate.

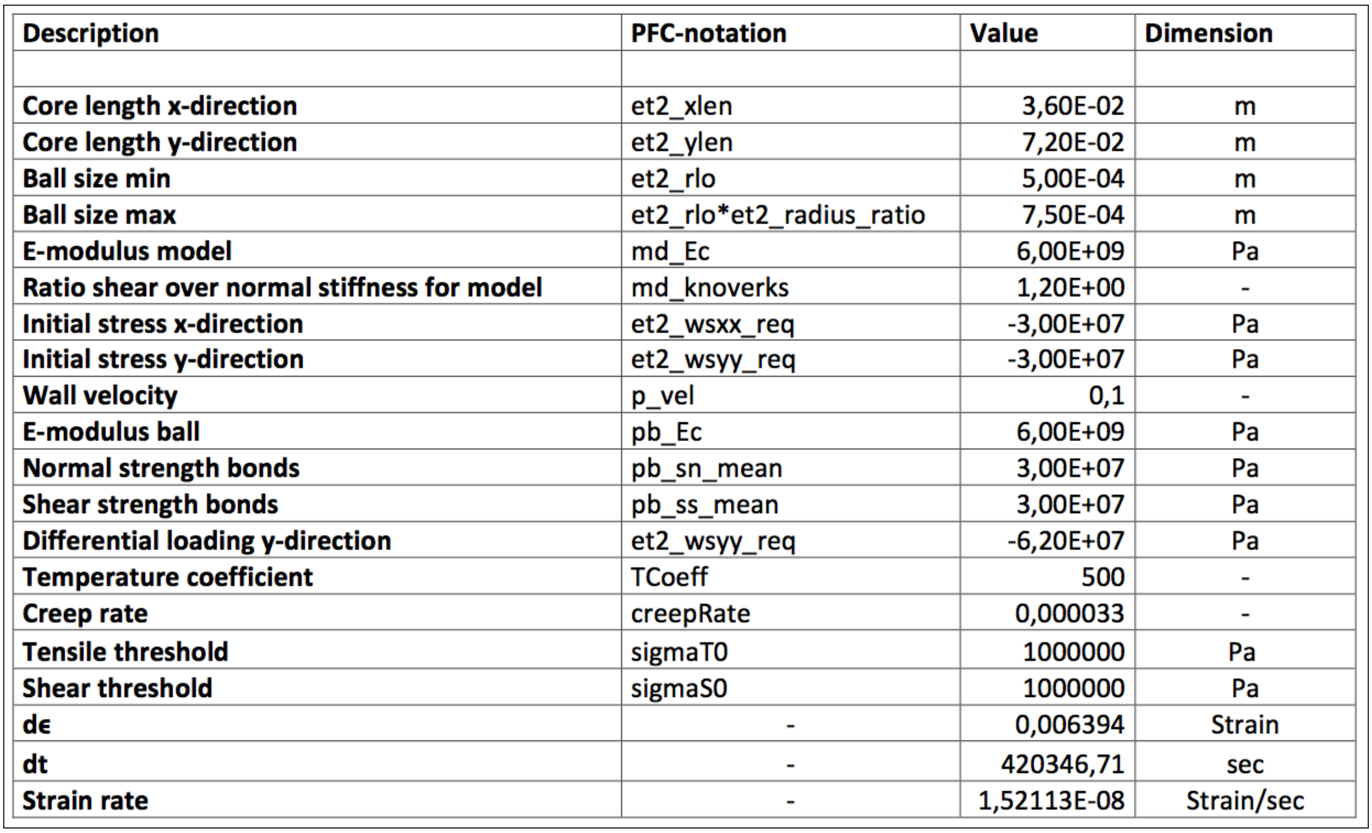

Description	**PFC-notation**	**Value**	**Dimension**
Core length x-direction	et2_xlen	3,60E-02	m
Core length y-direction	et2_ylen	7,20E-02	m
Ball size min	et2_rlo	5,00E-04	m
Ball size max	et2_rlo*et2_radius_ratio	7,50E-04	m
E-modulus model	md_Ec	6,00E+09	Pa
Ratio shear over normal stiffness for model	md_knoverks	1,20E+00	-
Initial stress x-direction	et2_wsxx_req	-3,00E+07	Pa
Initial stress y-direction	et2_wsyy_req	-3,00E+07	Pa
Wall velocity	p_vel	0,1	-
E-modulus ball	pb_Ec	6,00E+09	Pa
Normal strength bonds	pb_sn_mean	3,00E+07	Pa
Shear strength bonds	pb_ss_mean	3,00E+07	Pa
Differential loading y-direction	et2_wsyy_req	-6,20E+07	Pa
Temperature coefficient	TCoeff	500	-
Creep rate	creepRate	0,000033	-
Tensile threshold	sigmaT0	1000000	Pa
Shear threshold	sigmaS0	1000000	Pa
dϵ	-	0,006394	Strain
dt	-	420346,71	sec
Strain rate	-	1,52113E-08	Strain/sec

Figure 3.4: Key parameters in the core specimen simulation are presented as well as the PFC-notation and explanations.

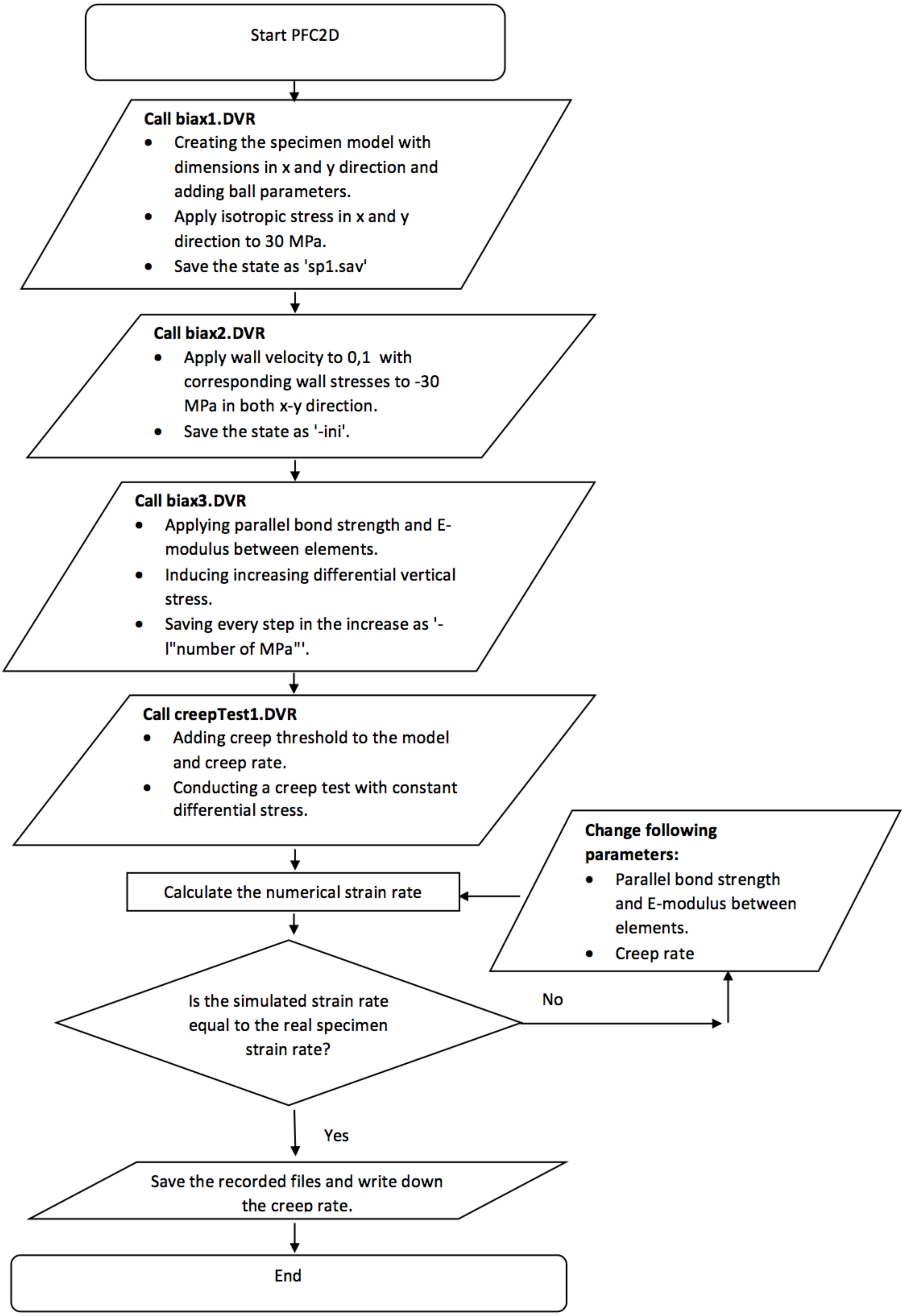

Figure 3.5: A simplified flowchart of the numerical calibration process.

All key parameters from the biaxial numerical calibration test are presented in figure 3.4. The bond strength between the elements is set to the lowest possible value before sufficient bonds in the specimen are broken. Such failure makes the numerical analysis invalid. It is also important to note that the creep threshold for both tensile and shear stress is set to 1 MPa in this initial simulation. The calibration of creep rates is presented in figure 3.6, and the grey figure denotes the creep rate 0,000033, which is required in order to achieve the real core specimen strain rate $1,5 * 10^{-8} s^{-1}$.

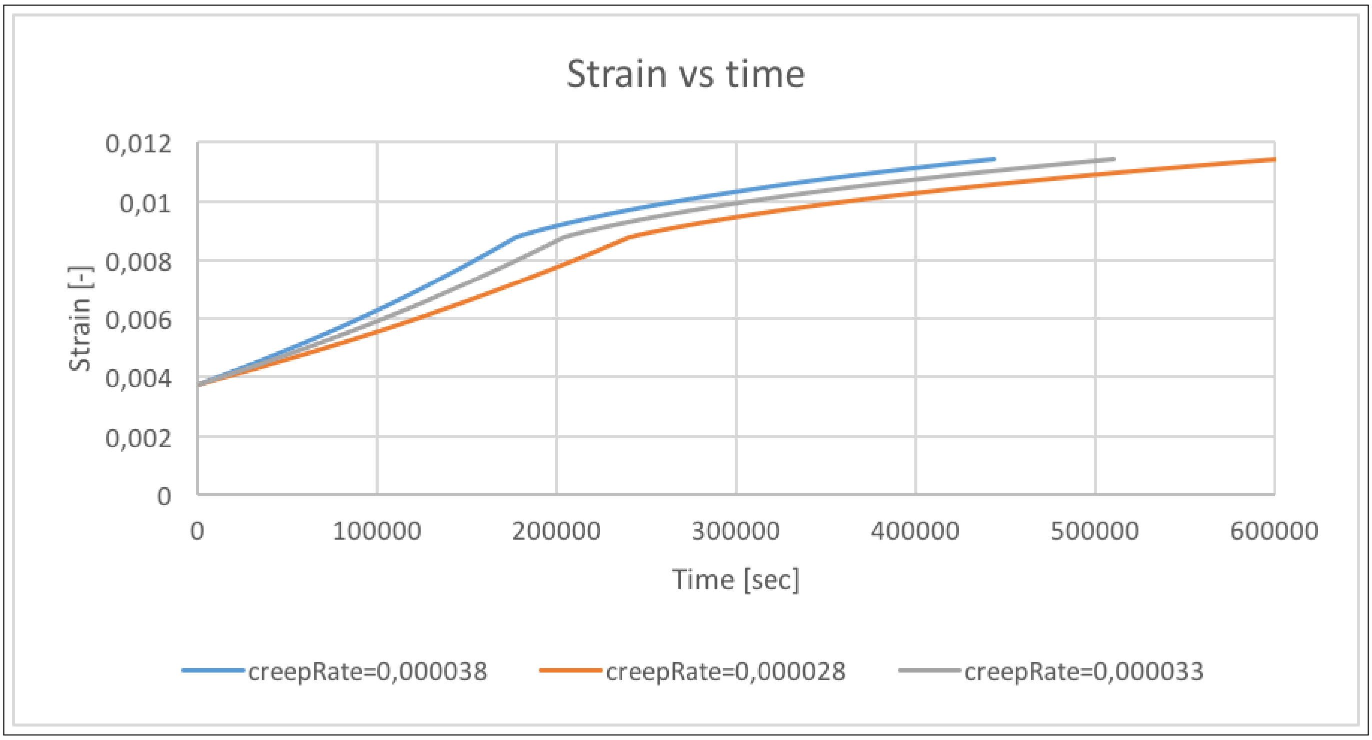

Figure 3.6: Strain as a function of time for different creep rates during the numerical strain rate calibration.

3.1.3 Evaluation of creep threshold for biaxial test

As described in section 2.1, the creep threshold stresses are important parameters for the numerical creep mechanism. It is therefore desided to investigate the impact this parameter has in the biaxial calibration test. The initial calibration test conducted in the previous section, calibrated the strain rate with a creep threshold on 1 MPa for both tensile strength and shear strength. By reducing threshold stresses to zero figure 3.7 shows there is no significant change in strain rate.

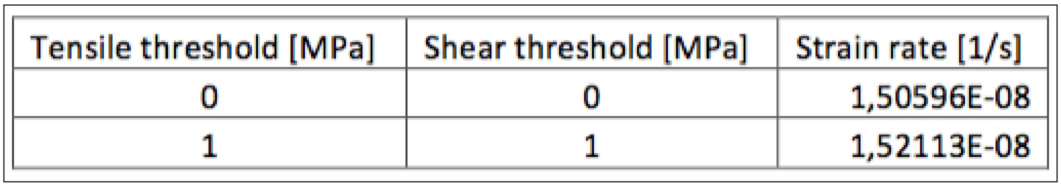

Tensile threshold [MPa]	Shear threshold [MPa]	Strain rate [1/s]
0	0	1,50596E-08
1	1	1,52113E-08

Figure 3.7: Different threshold stresses and corresponding strain rates.

3.2 Simulation of creep around a well

This section simulates a formation creeping around a borehole during a time period of approximately 1000 days. The simulations will involve visual monitoring and analysis on the stress distribution around the borehole through the development of the creep deformation. The parameters used and calibrated in section 3.1 apply in this borehole simulation. This includes of course the creep rate, 0,000033. Figure 3.8 presents the state right after the casing is set in a drilled borehole.

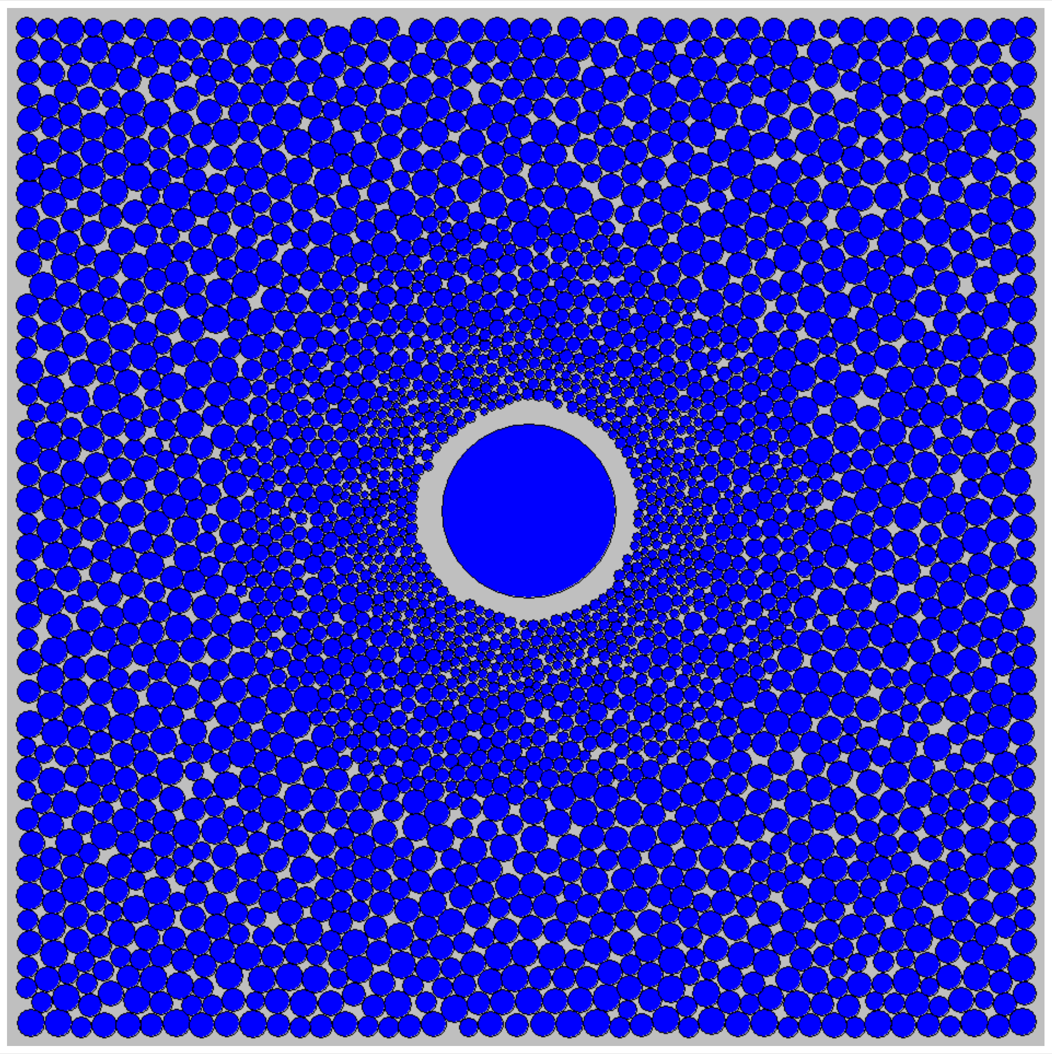

Figure 3.8: 2D ball plot of a vertical borehole right after casing is set.

3.2.1 Assumptions and simulation methodology

The following describes the downhole conditions which are simulated. A detailed PFC-technical description is presented in figure 3.9.

- The numerical simulations will mimic creep in a 17 1/2" (0,445 m) vertical borehole with a 13 3/8" (0,34 m) casing at 1000 m TVD.
- The well pressure $P_w = 0$ MPa and pore pressure $P_f = 0$ MPa (totally drained).
- The effective isotropic horizontal stress is 30 MPa.

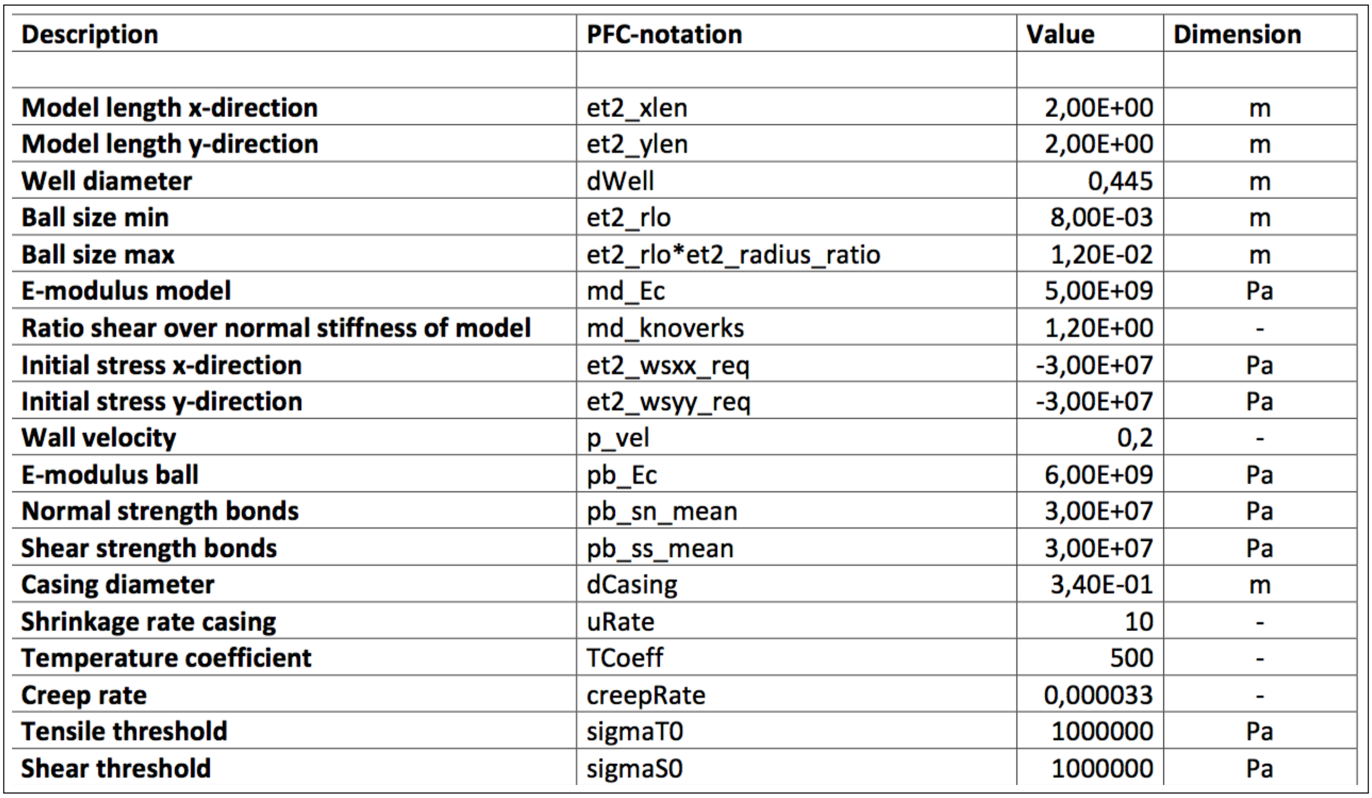

Description	**PFC-notation**	**Value**	**Dimension**
Model length x-direction	et2_xlen	2,00E+00	m
Model length y-direction	et2_ylen	2,00E+00	m
Well diameter	dWell	0,445	m
Ball size min	et2_rlo	8,00E-03	m
Ball size max	et2_rlo*et2_radius_ratio	1,20E-02	m
E-modulus model	md_Ec	5,00E+09	Pa
Ratio shear over normal stiffness of model	md_knoverks	1,20E+00	-
Initial stress x-direction	et2_wsxx_req	-3,00E+07	Pa
Initial stress y-direction	et2_wsyy_req	-3,00E+07	Pa
Wall velocity	p_vel	0,2	-
E-modulus ball	pb_Ec	6,00E+09	Pa
Normal strength bonds	pb_sn_mean	3,00E+07	Pa
Shear strength bonds	pb_ss_mean	3,00E+07	Pa
Casing diameter	dCasing	3,40E-01	m
Shrinkage rate casing	uRate	10	-
Temperature coefficient	TCoeff	500	-
Creep rate	creepRate	0,000033	-
Tensile threshold	sigmaT0	1000000	Pa
Shear threshold	sigmaS0	1000000	Pa

Figure 3.9: Key parameters in the borehole simulation are presented as well as the PFC-notation and explanations.

Figure 3.9 presents all the essential PFC-parameters required to replicate the creep around a borehole simulations in this report. Unlike figure 3.4, figure 3.9 includes the term uRate which is a parameter used to construct a virtual casing (figure 3.8); After the initial hole is constructed in the model and horizontal stress is applied, a hole-sized ball is placed inside the hole. The ball is then shrunk to the desired casing diameter. The rate of shrinkage is determined by the uRate, and it is important to be careful with this parameter. Too high uRate can induce dynamic effects which may result in break outs and undesirable crack development around the borehole. Too low uRate can result in no annulus development. This is because the induced horizontal stress and corresponding wall velocity may cause the borehole wall to move quicker towards the centre of the hole, than the shrinkage of the virtual casing. The creep threshold stresses are set to same as for the initial biaxial calibration test(sigmaS0=1 MPa and sigmaC0=1). There will be conducted analysis on different creep threshold stresses for borehole simulation later in the report.

Figure 3.10 presents the simulation methodology for how creep around a borehole is conducted. All parameters in figure 3.9 apply in the initial borehole simulation.

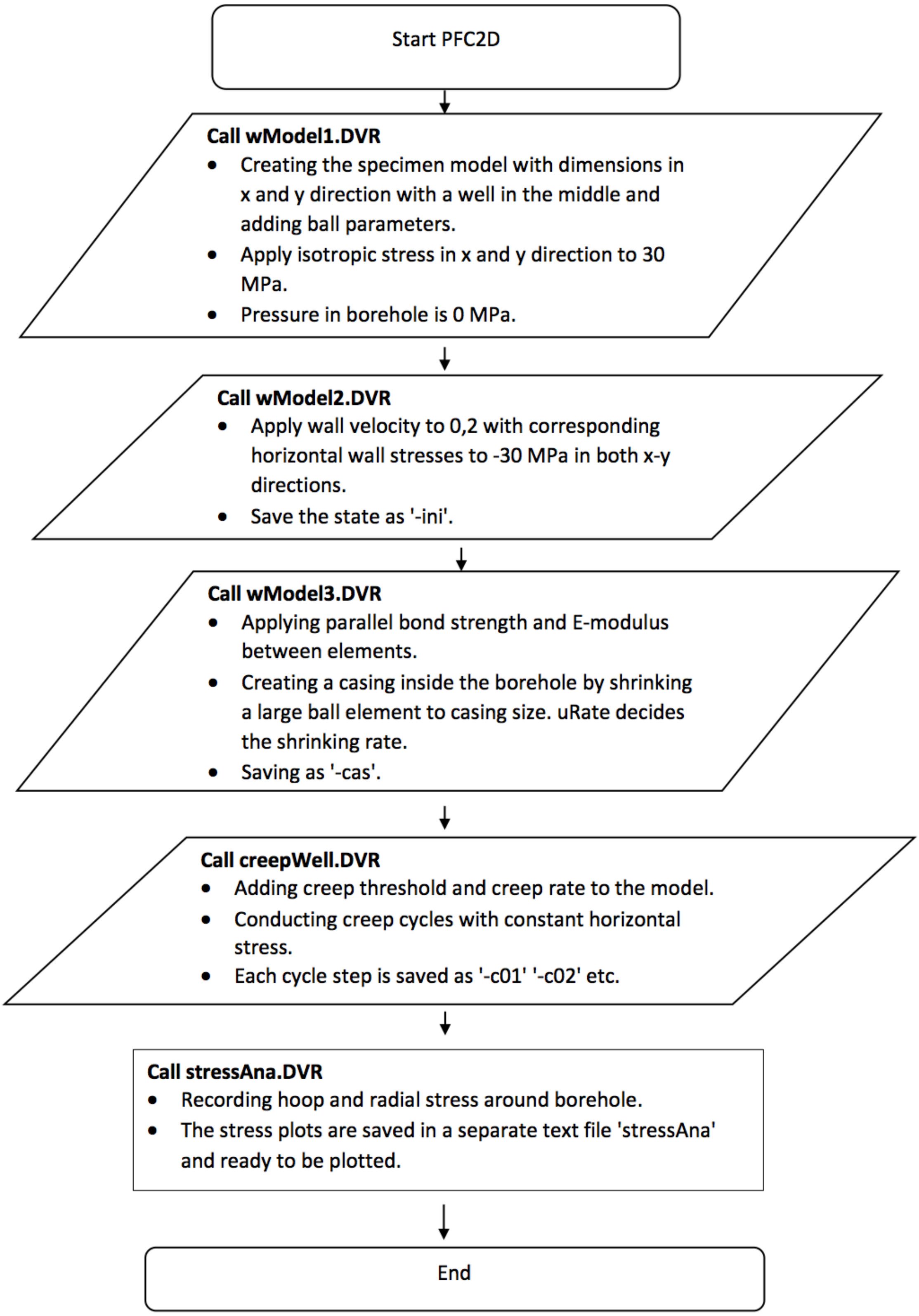

Call wModel1.DVR

- Creating the specimen model with dimensions in x and y direction with a well in the middle and adding ball parameters.
- Apply isotropic stress in x and y direction to 30 MPa.
- Pressure in borehole is 0 MPa.

Call wModel2.DVR

- Apply wall velocity to 0,2 with corresponding horizontal wall stresses to -30 MPa in both x-y directions.
- Save the state as '-ini'.

Call wModel3.DVR

- Applying parallel bond strength and E-modulus between elements.
- Creating a casing inside the borehole by shrinking a large ball element to casing size. uRate decides the shrinking rate.
- Saving as '-cas'.

Call creepWell.DVR

- Adding creep threshold and creep rate to the model.
- Conducting creep cycles with constant horizontal stress.
- Each cycle step is saved as '-c01' '-c02' etc.

Call stressAna.DVR

- Recording hoop and radial stress around borehole.
- The stress plots are saved in a separate text file 'stressAna' and ready to be plotted.

Figure 3.10: A simplified flowchart of the numerical creep around a borehole.

3.2.2 Borehole results with calibrated parameters and threshold stresses on 1 MPa

This section will present visual and graphical results of a formation creeping around a well for approximately 1000 days with the calibrated parameters in figure 3.9 applied. Figure 3.11 shows the initial state right after the virtual casing has shrunk to correct size. Although the creep mechanism is not yet induced, figure 3.11 indicates some break outs from the borehole wall, as some balls seem to have loosen during the shrinking process of the casing. Another observation to note is that the smallest balls have clustered near the borehole, while the larger balls are located further away from the well.

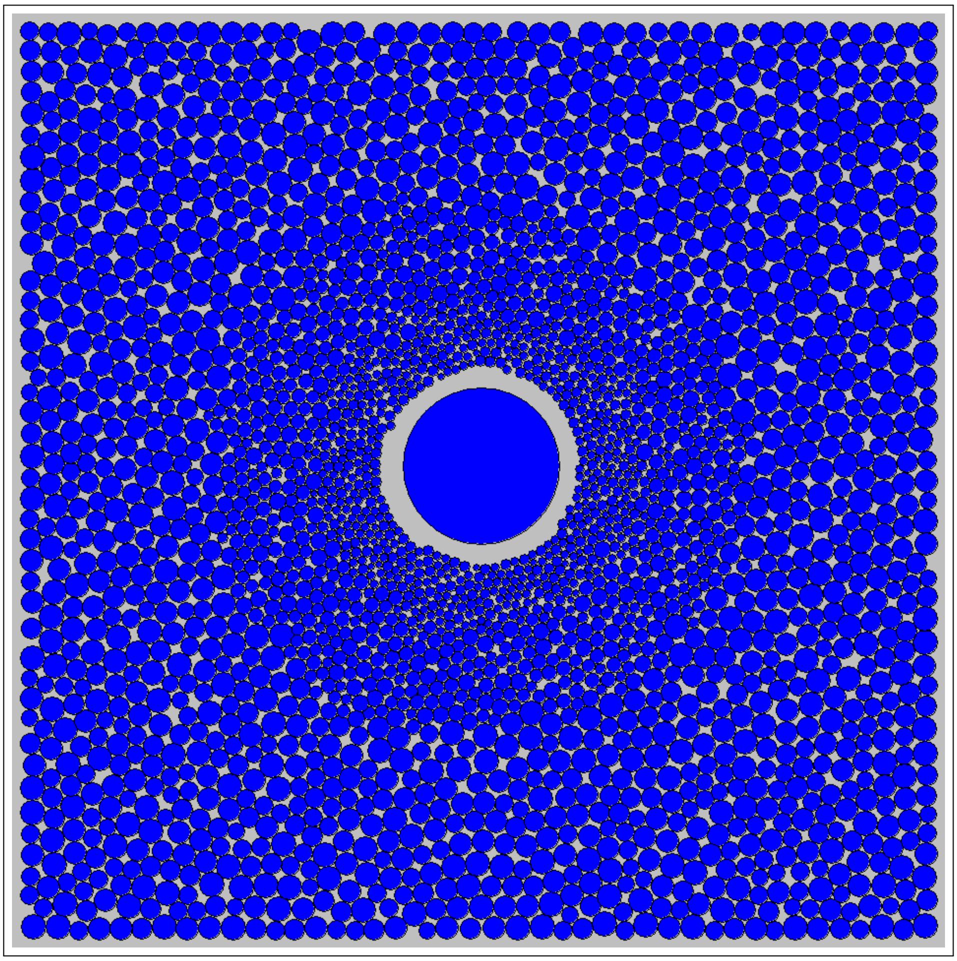

Figure 3.11: 2D ball plot of a vertical borehole at t=0.

Figure 3.12 presents the state of the borehole when the formation has been creeping for 277 days. The gap between casing and formation has narrowed and there are also indications of break outs. The locational distribution on ball sizes seems to be similar to the results in figure 3.11.

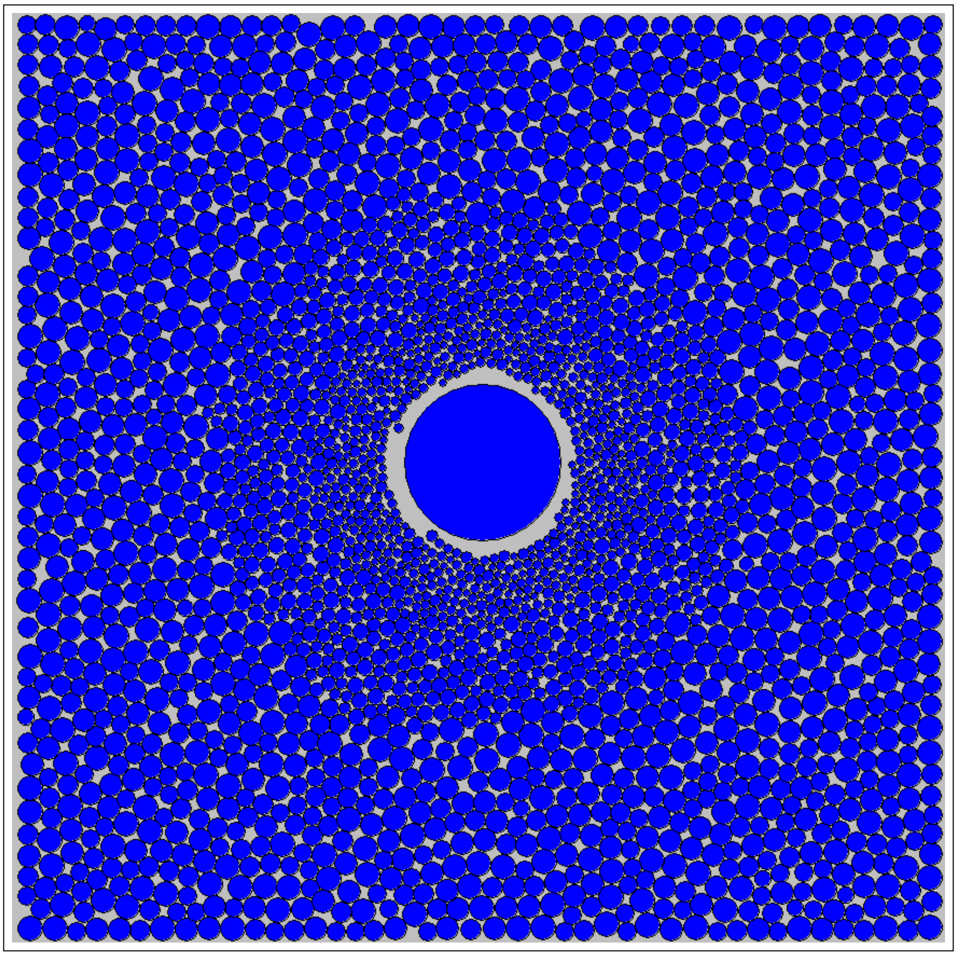

Figure 3.12: 2D ball plot of a vertical borehole at t=277.

Figure 3.13 gives a visual view of the situation when the formation has been creeping around a borehole for 1076 days. The gap has narrowed even more compared to t=277 days, and some places the formation has reached contact with casing.

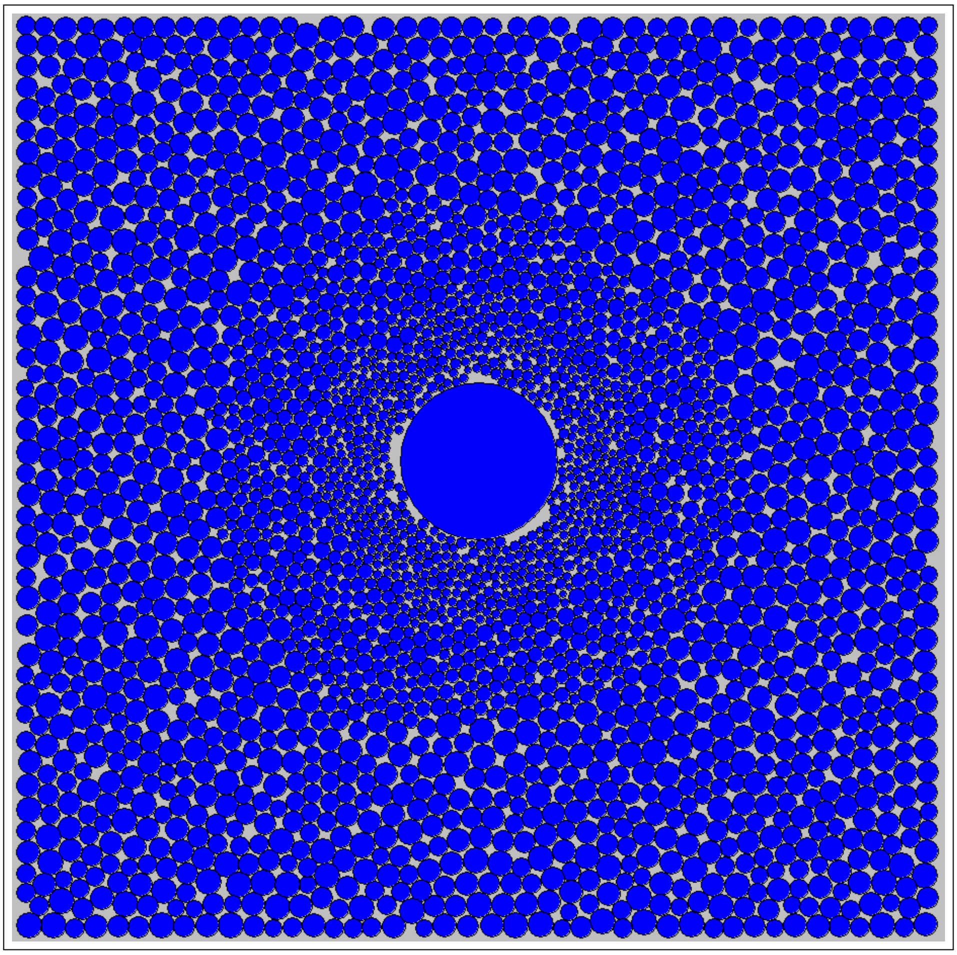

Figure 3.13: 2D ball plot of a vertical borehole at t=1076.

Figure 3.14 gives graphical results on the relative gap and relative pressure on casing. Relative gap is defined as the average reduced gap divided on the initial gap, while relative pressure is defined as ratio on the average pressure acting on casing over the applied horizontal stress on the model.

At t=0 days the gap has already narrowed approximately 20 % from its initial size. The figure also indicates that there are no pressure acting on the casing at this state. Further, the gap decreases and at t=277 days, it is reduced by approximately 50 % of its initial size. At around t=350 days, the relative pressure curve shows signs of contact between the formation and the casing.

The deformation rate decreases as these contacts are initiated and it reduces even more as the relative pressure starts to increase at approximately t=600 days. By the end, at t=1076, the average gap has narrowed to about 10 % of its original size, while the relative pressure on casing is about 15 % of the applied horizontal stress (0,15*30 MPa = 4,5 MPa).

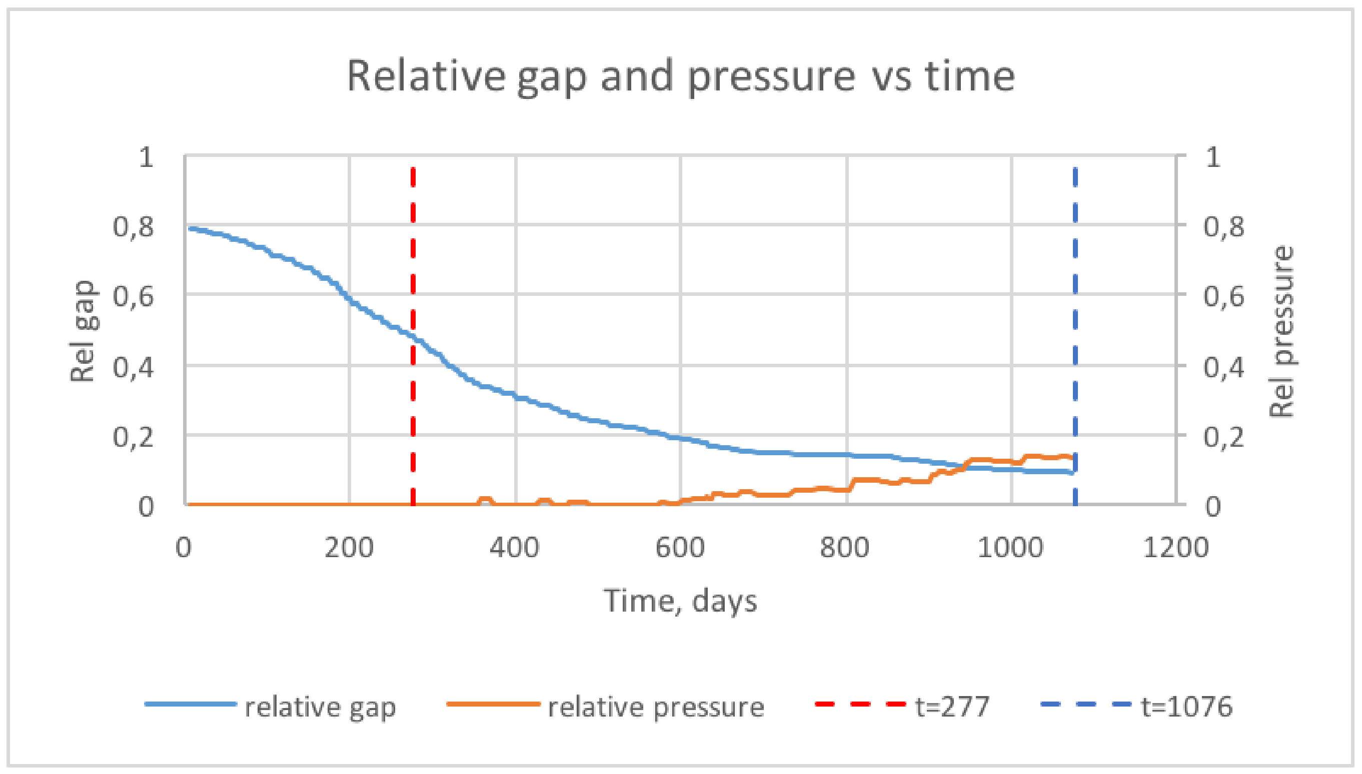

Figure 3.14: Relative gap and relative pressure on casing vs time.

Figure 3.15 presents the stresses around a borehole for the simulation above. The analysis conducted, are for both radial (sigmaR) and tangential (sigmaT) stresses around a borehole during creep through the time of 1076 days. The two dashed straight lines intersecting at (1, 30), indicates the initial well radius R and the horizontal far field stress (sigmaH) respectively. The stresses are evaluated for t=0, t=277 and t=1076. For t=0, the tangential stress peaks at the relative distance 2,225 from the wellbore with the magnitude on 65 MPa before it approaches the far field stress further in the formation. The tangential stress for t=277 peaks at the relative distance of approximately 2 from the wellbore with the magnitude of 35 MPa before it drops and starts approaching the far field stress. For t=1076, the tangential stress has a similar behaviour as for t=277. Figure 3.15 indicates that the radial stresses for all analysis, have a similar constant increase to the approach of far field stress.

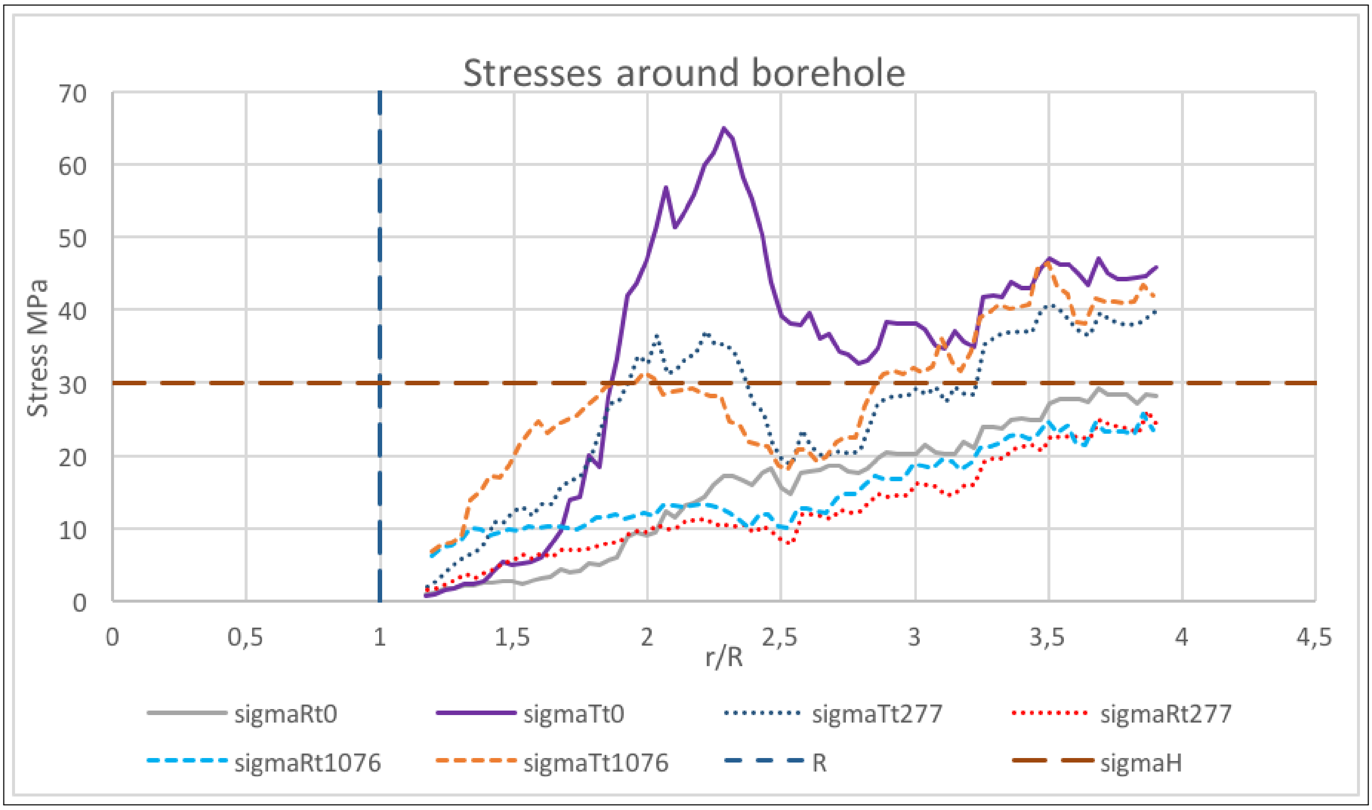

Figure 3.15: Tangential and radial stresses around a borehole during creep.

3.2.3 Borehole results with calibrated parameters and without threshold stresses

This section will present visual and graphical results of a formation creeping around a well for approximately 1000 days with the calibrated parameters applied in figure 3.9. The creep threshold stresses are not included which means sigmaT0=0 and sigmaS0=0. Figure 3.16 presents the initial state right after the casing has shrunk to its correct size. The borehole wall is smooth and the smaller balls are clustered near it, while the larger balls are located farther in the formation.

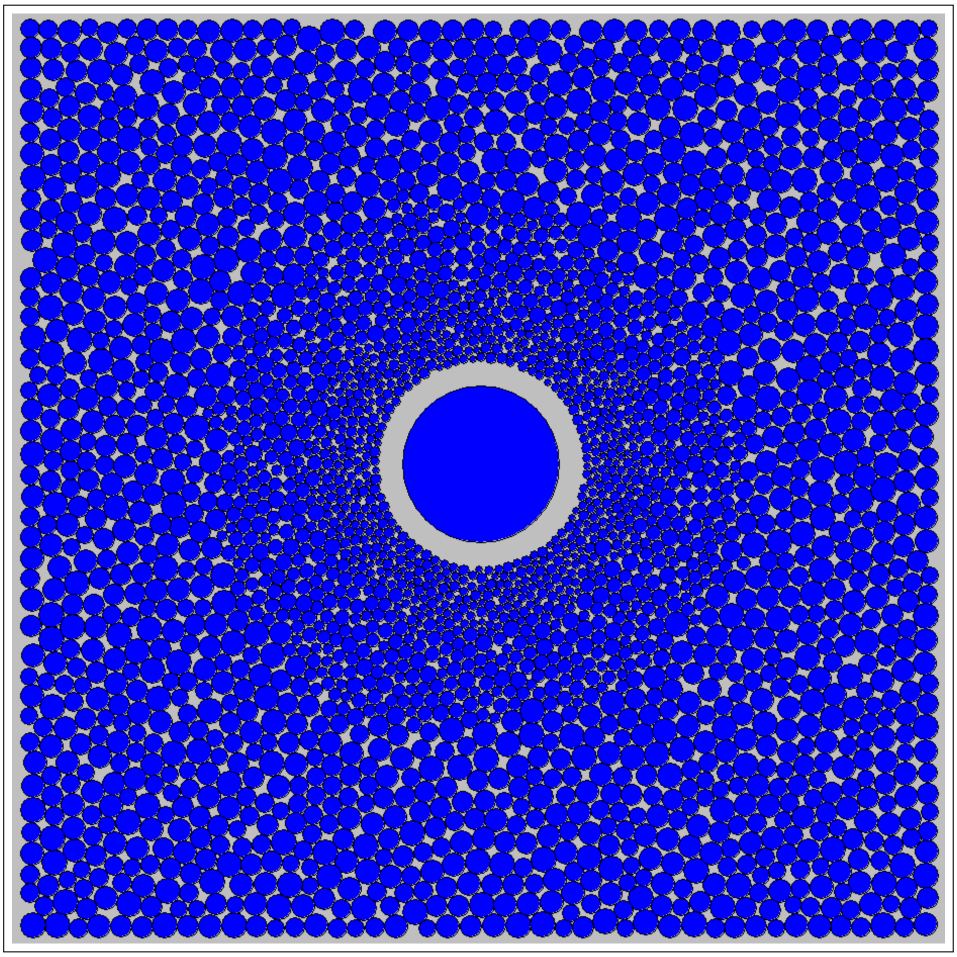

Figure 3.16: 2D ball plot of a vertical borehole at t=0.

Figure 3.17 shows the borehole state after t=360 days, and it indicates that the gap has narrowed. The formation has even in some regions managed to achieve contact with casing. The ball size distribution is the same as for t=0.

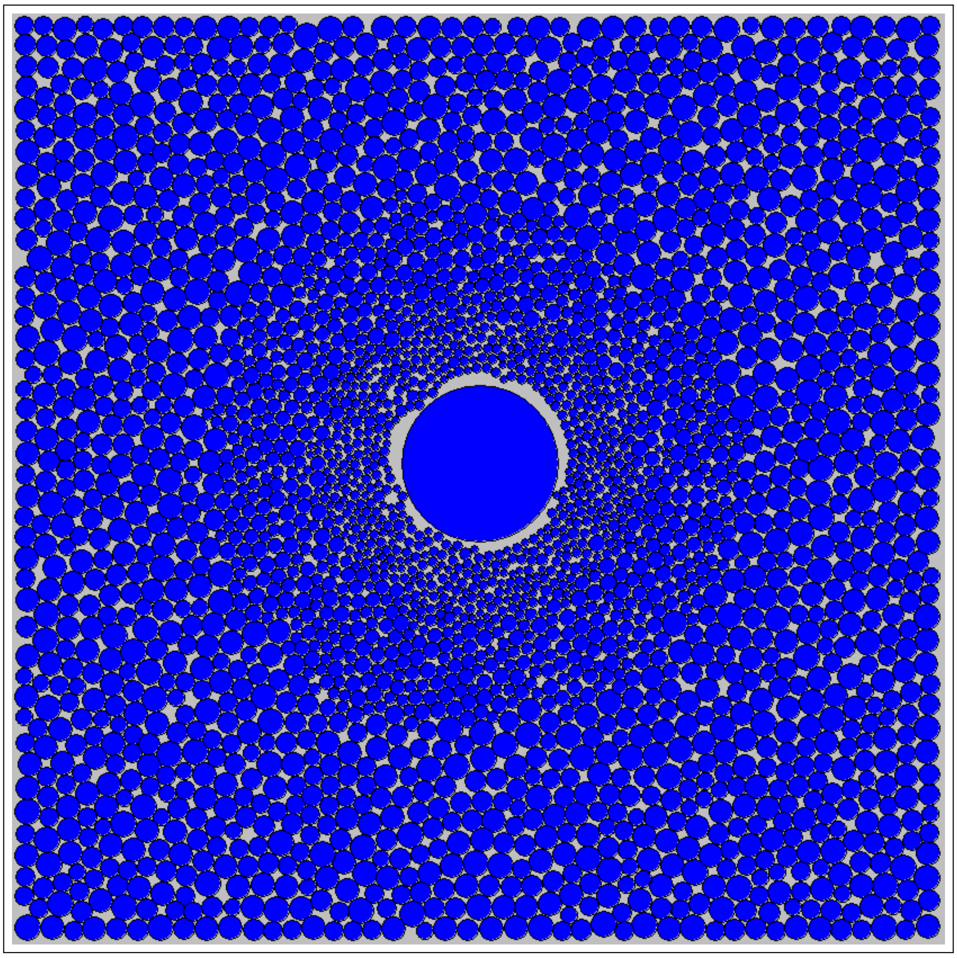

Figure 3.17: 2D ball plot of a vertical borehole at t=360.

The borehole state after t=1069 depicted in figure 3.18, presents a condition where the gap is almost vanished and the formation has reached more or less continously contact around the whole casing.

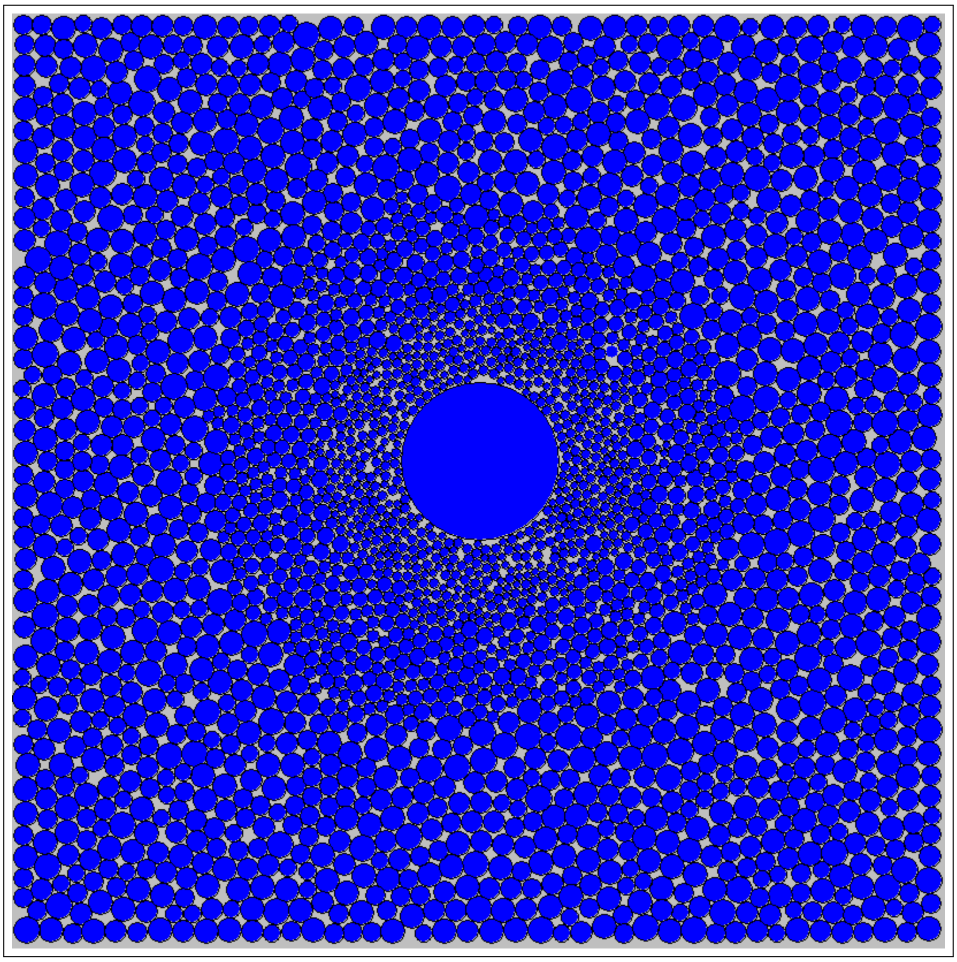

Figure 3.18: 2D ball plot of a vertical borehole at t=1069.

Figure 3.19 gives graphical results on the relative gap and relative pressure on casing. Relative gap is defined as the average reduced gap divided on the initial gap, while relative pressure is defined as ratio on the average pressure acting on casing over the applied horizontal stress on model.

Initially at t=0, relative gap is 100 % and the relative pressure on casing is zero percent. As the time goes on, the relative gap is steadily decreasing until contact force on casing is initiated (t=250 day). Now, the decline rate of relative gap is decreasing as the contact increases. At t=360, the relative gap has narrowed by approximately 70 % of its original gap size, while the relative average pressure acting on the casing has reached about 5 % of the far field horizontal stress (0,05*30 MPa = 1,5 MPa). Further, figure 3.19 shows that the average relative gap steadily decreases, while the average relative pressure on casing correspondingly increases. At t=1069, the average pressure is approximately 0,4* 30 MPa = 12 MPa, and the average gap is reduced to under 5 % of its initial size.

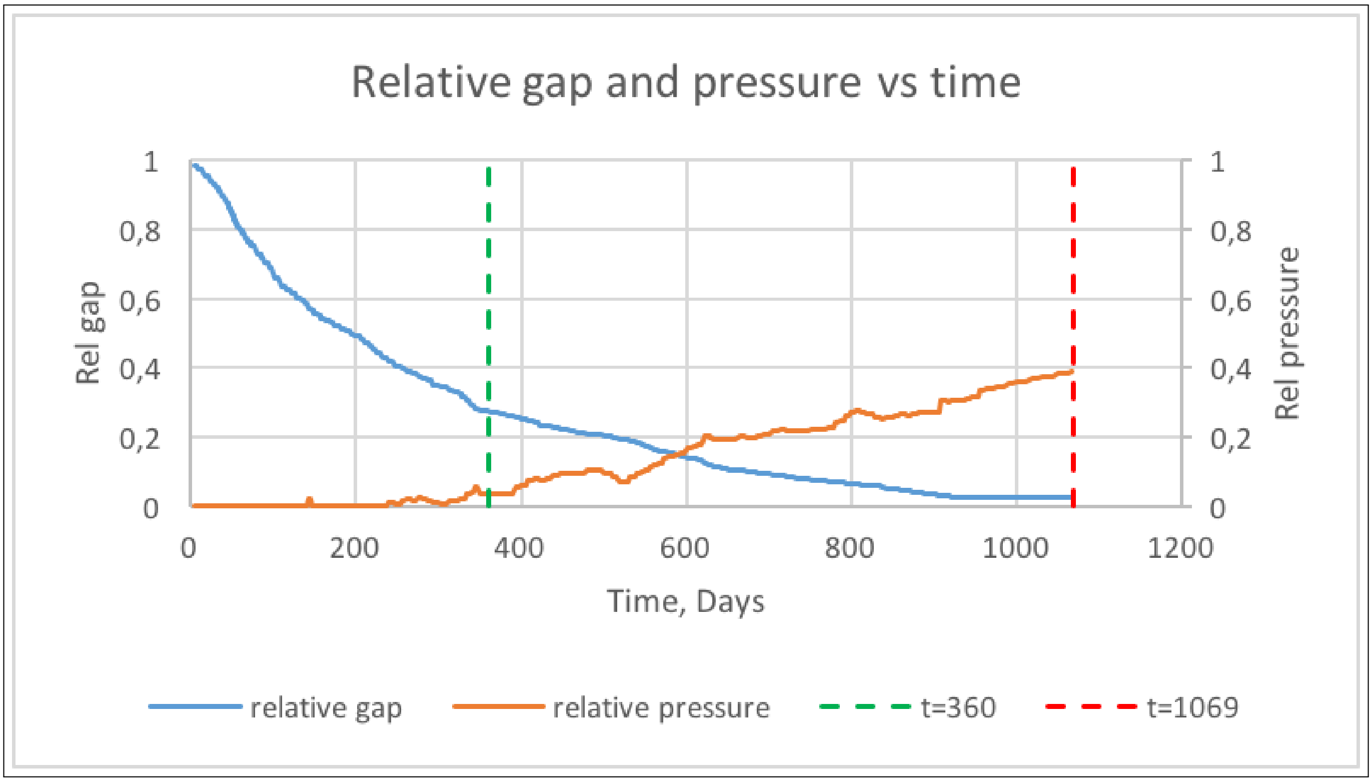

Figure 3.19: Relative gap and relative pressure on casing vs time.

Figure 3.20 presents the stresses around a borehole for the simulation above. The analysis conducted, are for both radial (sigmaR) and tangential (sigmaT) stresses around a borehole during creep through the time of 1069 days. The two dashed straight lines intersecting at (1, 30), indicates the initial well radius R and the horizontal far field stress (sigmaH) respectively. The stresses are evaluated for t=0, t=360 and t=1069. For t=0, the tangential stress peaks at the relative distance approximately 2 from the wellbore with the magnitude on 38 MPa before it drops below the horizontal stress and then finally approaches the far field stress farther in the formation. The tangential stress for t=360 peaks at the relative distance of approximately 2 from the wellbore with the magnitude of 44 MPa before it drops and starts approaching the far field stress. For t=1069, the tangential stress has a similar behaviour as for t=277. Figure 3.20 indicates that the radial stresses for all analyses, except for t=0, have a similar constant increase to the approach of far field stress. The radial stress for t=0 have a constant increase greater than for t=360 and t=1069 until it exceeds the horizontal stress. Then it drops before it starts to approach the far field horizontal stress.

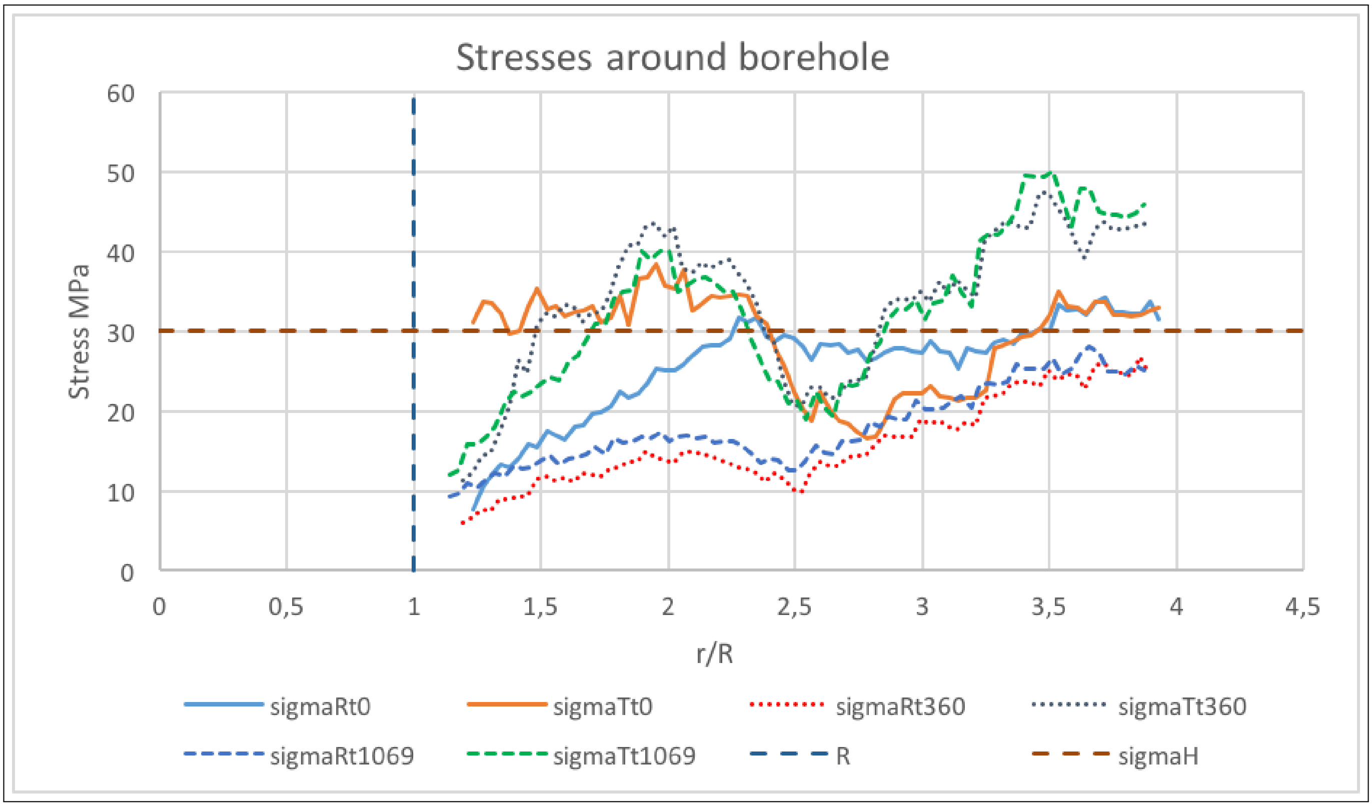

Figure 3.20: Tangential and radial stresses around a borehole during creep.

4 Plastic strain deformation

Plasticity is often used to describe the behaviour of a rock beyond failure. The rock's behaviour at this state is non-linear, and deformation does not recover when the load causing the deformation ceases. Figure 4.1 describes a stress-strain situation where a rock contains linear elastic and ideal plastic material. The figure shows that initially, the rock undergoes a linear elastic deformation until it reaches the yield point. At this point, the rock initiates a plastic deformation which increases with constant load. This describes an ideal plastic behaviour which will be assumed in derivation and theory throughout this section.

In this report, the term plastic strain deformation will not include time. This is a likely assumption as the rock has reached the state of equilibrium when referring to this phenomenon. Creep is also a deformation phenomenon which may reach steady state with sufficient time. This makes it difficult to distinguish the difference between the two deformations. Although this section refers to deformation as plastic strain, one should not exclude that the deformation also can be a result of creep.

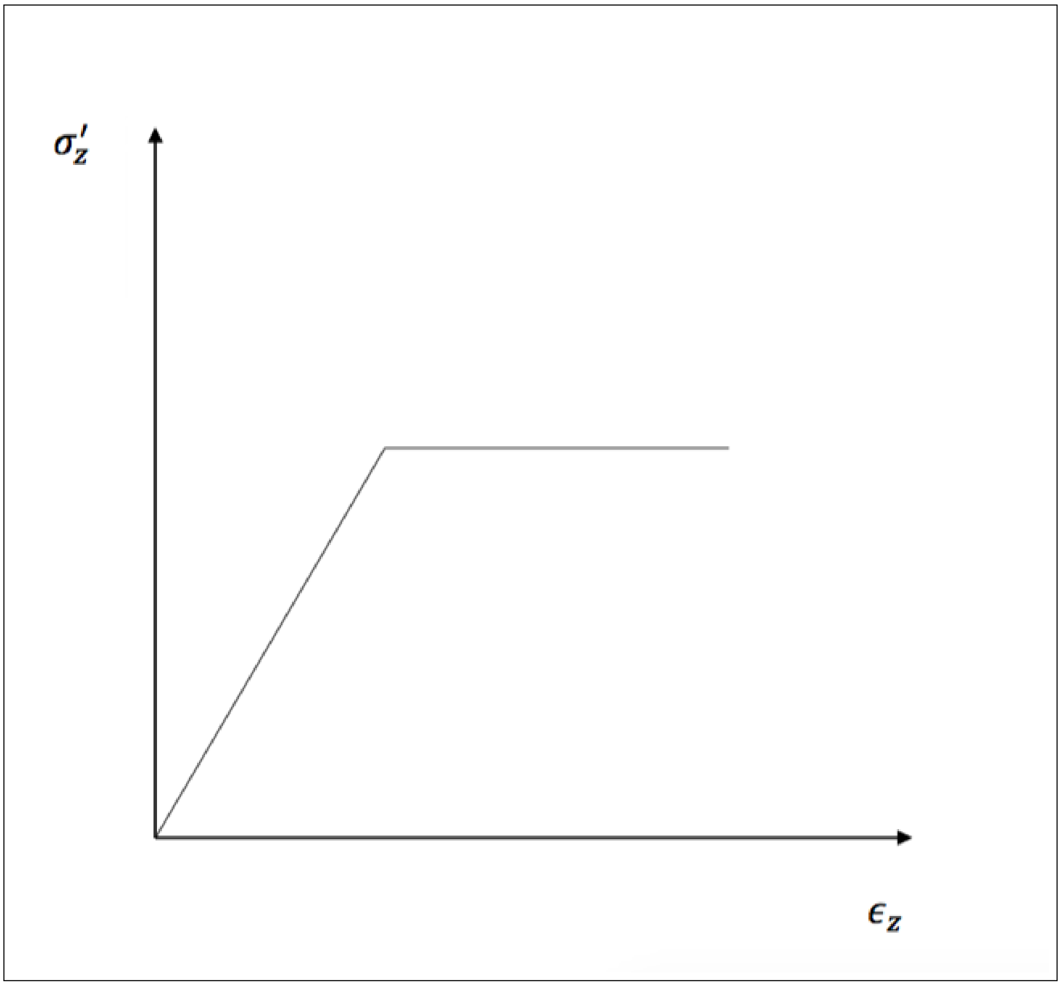

Figure 4.1: Stress-strain curve for linear plastic and ideally plastic material.

4.1 Stresses around a borehole with Mohr-Coulomb criterion

Stability of a borehole after failure can be described analytically by the Mohr-Coulomb criterion. The failure is explained as a transition from elastic to plastic behaviour, which by Mohr-Coulomb involves a friction angle as well as rock strength. Unlike (Skomedal, 2015) [5], the derivation in this report allows the friction angle and rock strength to alter when the rock behaviour is transited from elastic to the plastic state. The ideal plasticity still applies by allowing the altered parameter, but there will be some discontinuity in the transition from elasticity to plasticity. This issue is going to be elaborated in section 4.2. Further, the derivation assumes that the vertical stress $\sigma_v = 0$ and the pore pressure $P_f = 0$. These simplifications make σ_r and σ_θ the only principal stresses as well as the effective stress is equal to the total stress; ${\sigma'}_{r,\theta} = \sigma_{r,\theta}$. With $\sigma_\theta > \sigma_r$, the Mohr-Coulomb criterion is written as following:

$$\sigma_\theta = C_0 + \sigma_r \tan^2 \beta \tag{4.1}$$

By allowing altered plastic parameters, eq. 4.1 gives:

$$\sigma_\theta = C_0^* + \sigma_r \tan^2 \beta^* \tag{4.2}$$

C_0^* is in this thesis referred to as unconfined residual strength and β^* is the altered friction angle after elastic-plastic transition. Further, for simplicity $\tan^2 \beta^* = k^*$. Hence:

$$\sigma_\theta = C_0^* + k^* \sigma_r \tag{4.3}$$

Introducing the equilibrium equation:

$$\frac{\delta \sigma_r}{\delta r} + \frac{\sigma_r - \sigma_\theta}{r} = 0 \tag{4.4}$$

Inserting eq. (4.3) into the equilibrium equation (4.4) gives:

$$\frac{\delta \sigma_r}{\delta r} + \frac{\sigma_r (1 - k^*)}{r} = \frac{C_0^*}{r} \tag{4.5}$$

Solving this differential equation with respect on σ_r in the plastic region and the boundary condition $\sigma_r(R) = P_w$ yields:

$$\sigma_r = \left(P_w + \frac{C_0^*}{k^* - 1}\right)\left[\frac{r}{R}\right]^{k^*-1} - \frac{C_0^*}{k^* - 1} \tag{4.6}$$

For the hoop stress in the plastic zone, substituting eq. (4.6) into the Mohr-Coulomb criterion (4.3) gives:

$$\sigma_\theta = k^*\left(P_w + \frac{C_0^*}{k^* - 1}\right)\left[\frac{r}{R}\right]^{k^*-1} - \frac{C_0^*}{k^* - 1} \tag{4.7}$$

The two equations above eq. (4.6) and eq. (4.7) only relates to the plastic zone. As for the region $r > R_p$, elastic properties rules, and the fact that $\sigma_r = \sigma_\theta$ far from the borehole gives:

$$\sigma_r = \sigma_h - \frac{C_2^{'}}{r^2} \tag{4.8}$$

and

$$\sigma_\theta = \sigma_h + \frac{C_2^{'}}{r^2} \tag{4.9}$$

Adding these equation yields:

$$\sigma_\theta = 2\sigma_h - \sigma_r \tag{4.10}$$

Which is the hoop stress on the borehole wall. Inserting this into the Mohr-Coulomb criterion eq. (4.1) in elastic state yields radial stress at the elastic-plastic boundary:

$$\sigma_r(R_p) = \frac{2\sigma_h - C_0}{k + 1} \tag{4.11}$$

The plastic zone radius is found by inserting eq. (4.11) into eq. (4.6) and set $r = R_p$:

$$\frac{R_p}{R} = \left[\frac{2\sigma_h - C_0 + (k+1)\frac{C_0^*}{k^*-1}}{(P_w + \frac{C_0^*}{k^*-1})(k+1)}\right]^{\frac{1}{k^*-1}} \tag{4.12}$$

It is now possible to find the coefficient C_2'. Inserting eq. (4.12) into eq. (4.8) with $r = R_p$ yields:

$$C_2' = R_p^2(\sigma_h - \sigma_r(R_p)) \tag{4.13}$$

4.2 Explanation and review of altered plastic parameters

The derivation of the Mohr-Coulomb in the previous section, considered that the plastic parameters could alter when rock behaviour changed from elastic to plastic. A triaxial test (figure 4.2) can be used to make an easy understandable analogy, although the main application to this theory is related to boreholes.

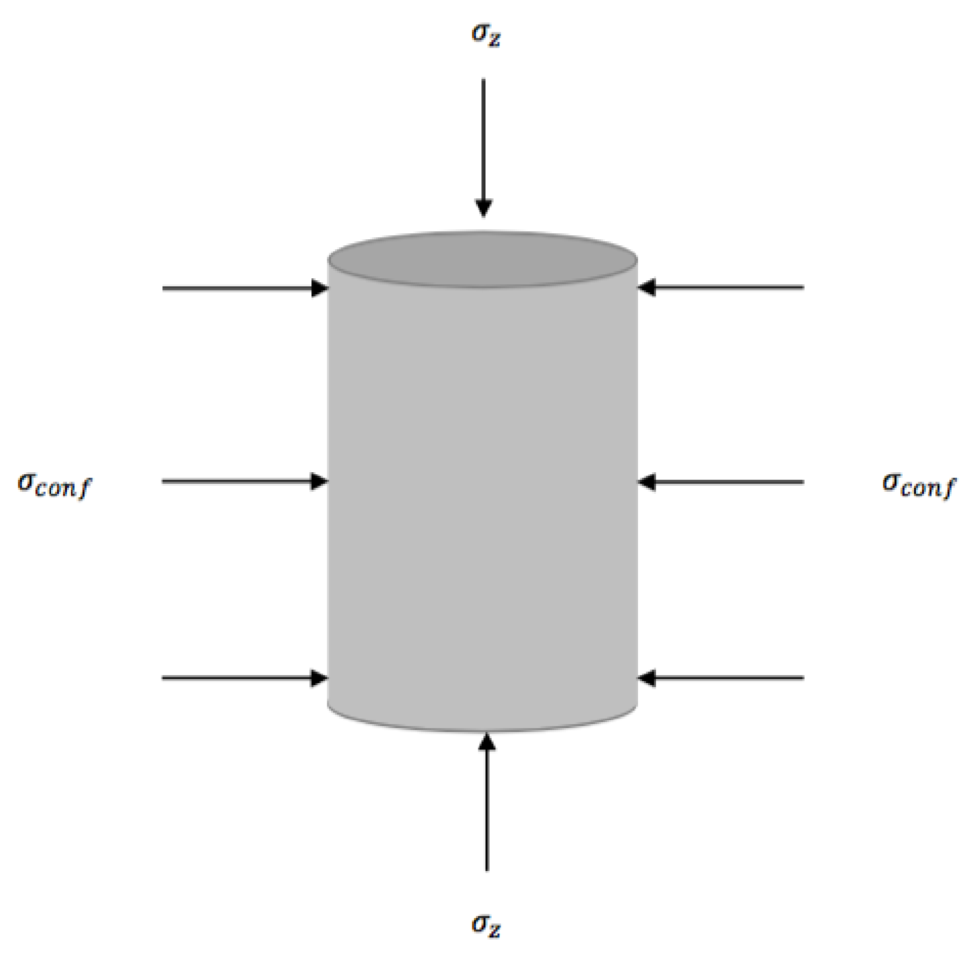

Figure 4.2: Triaxial test with confining stress and loading stress.

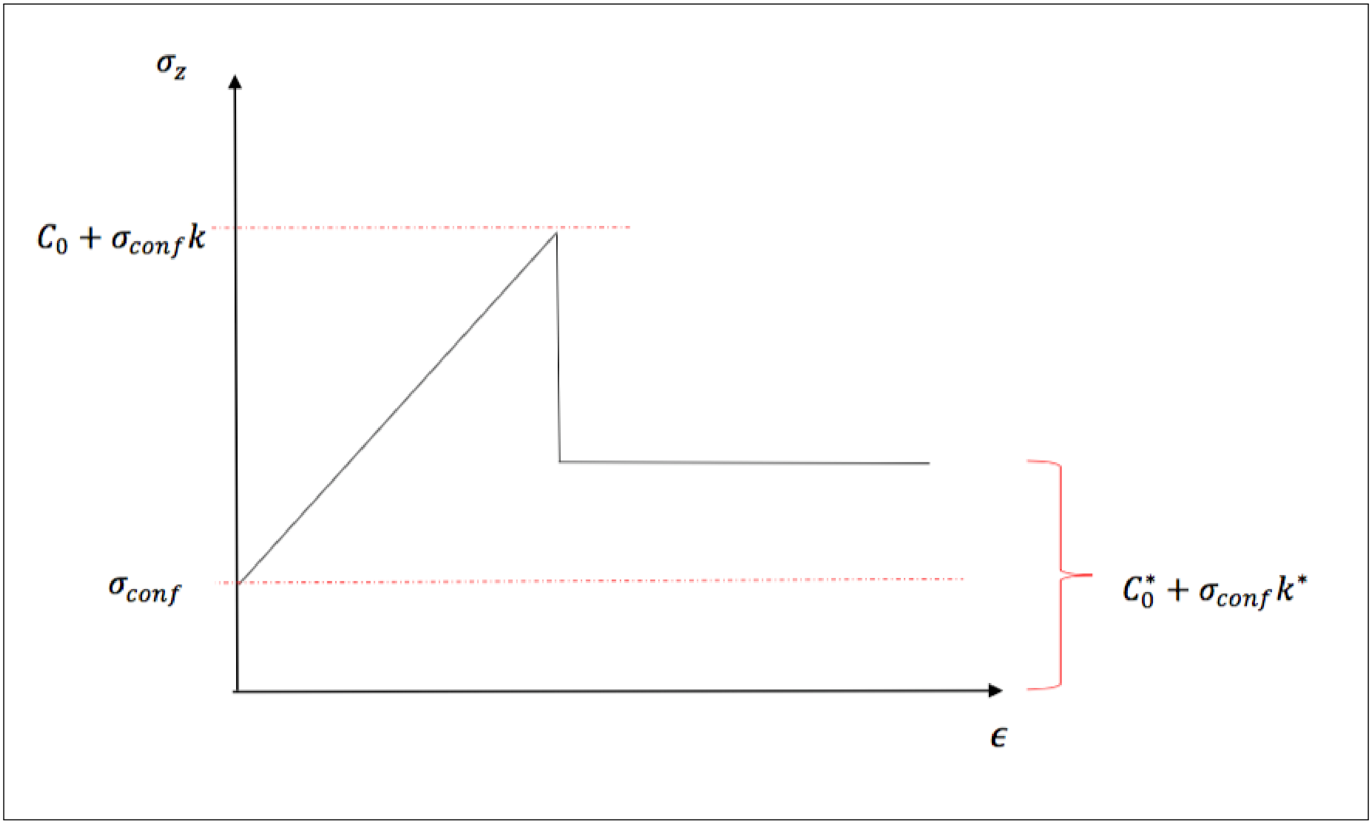

Figure 4.3: A graph of a triaxial test with confining stress and loading stress as a function of strain.

Figure 4.3 gives a qualitatively graphical presentation of the triaxial test illustrated in figure 4.2. The core specimen undergoes an increasing load in the vertical direction σ_z until peak stress. According to Mohr-Coulomb, this is where the rock fails and moves over from an elastic to a plastic behaviour. The stress at this point is a function of $C_0 + \sigma_{conf} k$ as denoted in figure 4.3. Beyond the point of failure, as the rock has reached a plastic behaviour, both k and C_0 transfers to k^* and an C_0^* respectively. This transition is conventionally referred to the term softening, which in reality give a less declining behaviour depending on the brittleness of the material (Brady et al, 1973) [14]. The model in this report does not involve this declining behaviour as it drops directly to the equilibrium state where it still has an ideal plastic behaviour. The strength at this state is referred to residual strength and is a function of $C_0^* + \sigma_{conf} k^*$. The impact of this residual strength is going to be discussed later in the report. Also note that both k^* and C_0^* can never exceed k and C_0 according to Mohr-Coulomb.

k^*-determination

The new friction constant k^* can be determined by recording C_0^* as a function of increasing confining pressure presented in figure 4.4. The friction coefficient is calculated from the slope determined by linear regression of the recorded data. The following presents how to calculate the new altered friction angle and the corresponding friction constant:

The slope is given by:

$$n^* = \frac{\Delta AFS^*}{\Delta \sigma^*_{conf}} \tag{4.14}$$

The friction coefficient (Sone and Zoback, 2013) [15]:

$$\mu^* = \frac{n^* - 1}{2\sqrt{n^*}} \tag{4.15}$$

The friction angle:

$$\phi^* = tan^{-1}\mu^* \tag{4.16}$$

The angle relation:

$$\beta^* = \frac{\pi}{4} + \frac{\phi^*}{2} \tag{4.17}$$

Which leads tho the new friction constant:

$$k^* = tan^2\beta^* \tag{4.18}$$

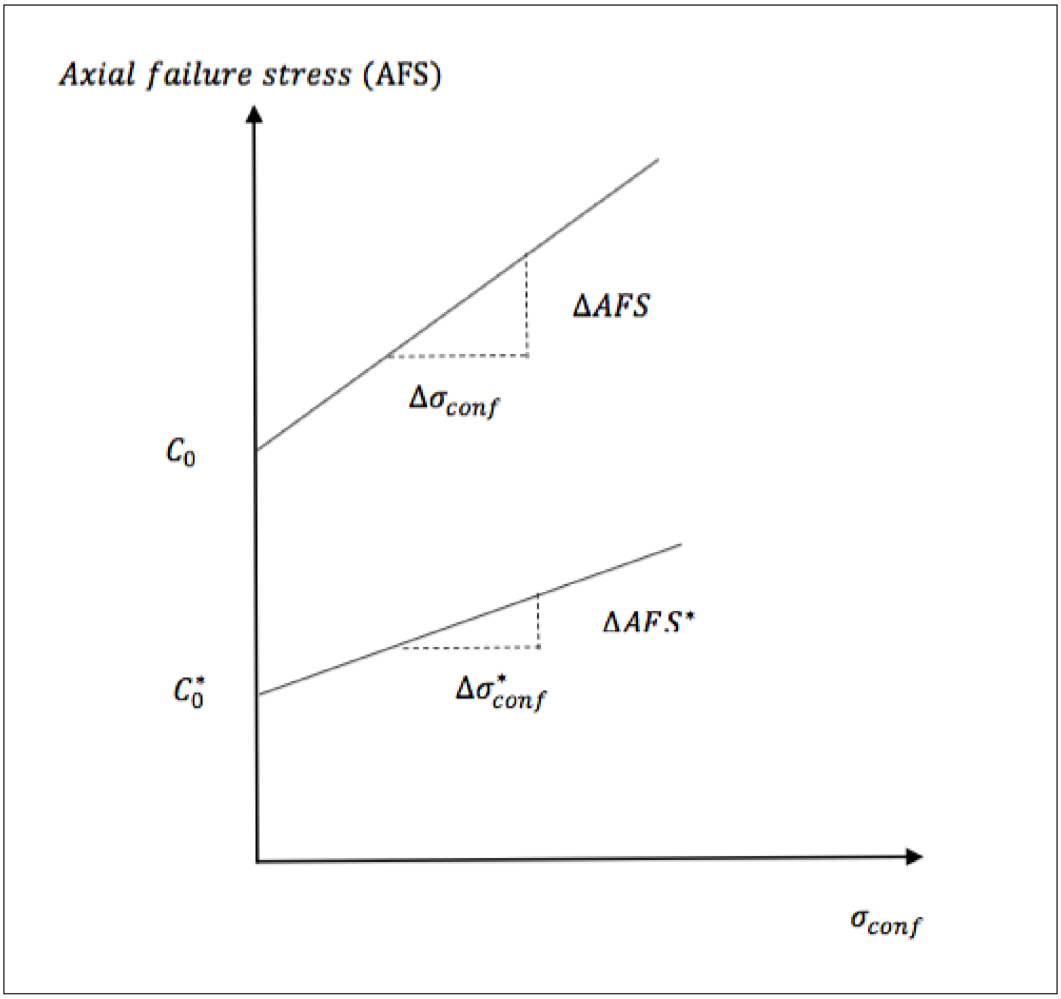

Figure 4.4: Axial failure stress as a function of confining pressure.

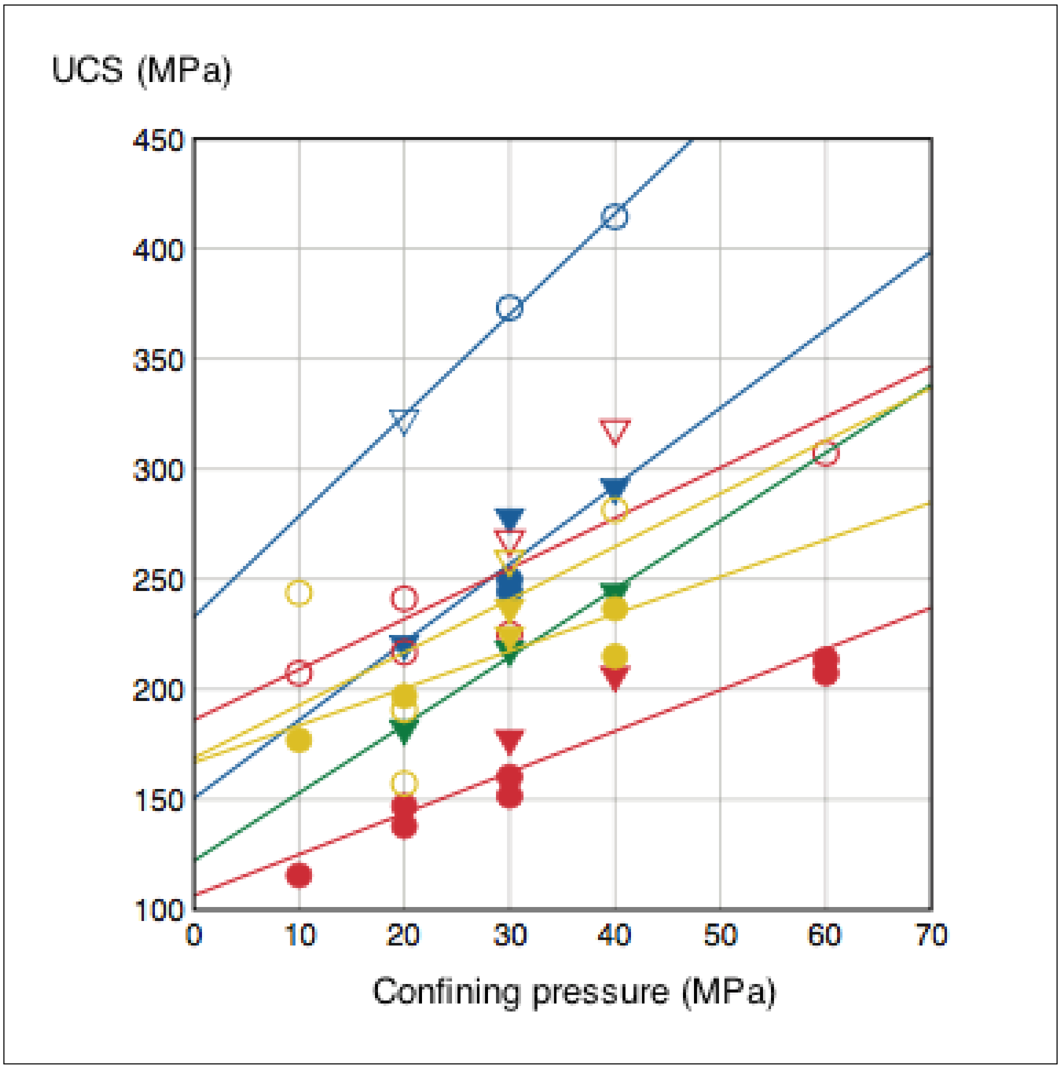

Figure 4.5: (Sone and Zoback, 2013) [15] Uniaxial compressive strength as a function of confining pressure for different shales.

4.3 Plastic and elastic stain deforamtion with the Mohr-Coulomb criterion

This section concerns plastic and elastic strain deformation around a borehole with the Mohr-Coulomb criterion described in section 4.1. Long term plasticity around well bore gives a totally drained condition. This makes the Mohr-Coulomb criterion suitable as it applies under this condition. The method used in the following calculations is inspired by the Tresca approach in (Fjær et al, Ch. 4, 2008) [7] but with different boundary conditions. It also includes the possibility for altered plasticity parameters introduced in the previous sections. Similar work is also been done in (Risnes et al, 1982) [16]. The following derivation is conducted by Erling Fjær and Øyvind Skomedal.

The Mohr-Coulomb criterion with altered plastic parameters is written as following:

$$f(\sigma'_r, \sigma'_\theta) = \sigma'_\theta - k^*\sigma'_r - C_0^* = 0 \tag{4.19}$$

Where k^* is the friction factor $tan^2\beta^*$ in the plastic state.

The plastic strains with the associated flow rule are

$$\epsilon_r^p = d\lambda_p \frac{\delta f}{\delta \sigma_r} = -k^* d\lambda_p \tag{4.20}$$

$$\epsilon_\theta^p = d\lambda_p \frac{\delta f}{\delta \sigma_\theta} = d\lambda_p \tag{4.21}$$

From the definition of total strain, relations between displacement and effective stresses in porous permeable formations give:

$$\sigma'_r = (\lambda + 2G)\Big[\frac{\delta u}{\delta r} + k^* d\lambda_p\Big] + \lambda\Big[\frac{u}{r} - d\lambda_p\Big] \tag{4.22}$$

and

$$\sigma'_\theta = (\lambda + 2G)\Big[\frac{u}{r} - d\lambda_p\Big] + \lambda\Big[\frac{\delta u}{\delta r} + k^* d\lambda_p\Big] \tag{4.23}$$

Substituting eq. 4.22 and 4.23 into eq. 4.19 and solve for $d\lambda_p$ gives:

$$d\lambda_p = \frac{\frac{u}{r}(\lambda+2G) - k^*\frac{\delta u}{\delta r}(\lambda+2G) + \lambda\Big[\frac{\delta u}{\delta r} - k^*\frac{u}{r}\Big] - C_0^*}{(\lambda+2G)(k^{*2}+1) - 2k^*\lambda} \tag{4.24}$$

λ+$2G$ is substituted with H (uniaxial compaction modulus) and $\frac{1}{H(k^{*2}+1)-2k^*\lambda} = q$. Thus:

$$d\lambda_p = -q\Big[-\frac{u}{r}(H-\lambda k^*) + \frac{\delta u}{\delta r}(Hk^* - \lambda) + C_0^*\Big] \tag{4.25}$$

The stresses in eq. 4.23 and 4.24 is then:

$$\sigma'_r = A_r + B_r\frac{\delta u}{\delta r} + C_r\frac{u}{r} \tag{4.26}$$

$$\sigma'_\theta = A_\theta + B_\theta\frac{\delta u}{\delta r} + C_\theta\frac{u}{r} \tag{4.27}$$

where

$$A_r = qC_0^*(Hk^* - \lambda) \tag{4.28}$$

$$B_r = H - q(Hk^* - \lambda)^2 \tag{4.29}$$

$$C_r = \lambda + q(Hk^* - \lambda)(H - \lambda k^*) \tag{4.30}$$

$$A_\theta = qC_0^*(H - \lambda k^*) \tag{4.31}$$

$$B_\theta = C_r \tag{4.32}$$

$$C_\theta = H - q(H - \lambda k^*)^2 \tag{4.33}$$

The equilibrium equation:

$$\frac{\delta \sigma_r}{\delta r} + \frac{\sigma_r - \sigma_\theta}{r} \tag{4.34}$$

Inserting the effective stresses eq. 4.26 and 4.27 into equilibrium eq. 4.34 gives:

$$\frac{\delta^2 u}{\delta r^2} + \frac{1}{r}\frac{\delta u}{\delta r} - \frac{C_\theta}{B_r}\frac{u}{r^2} + \frac{A_r - A_\theta}{rB_r} + \frac{\alpha}{B_r}\frac{\delta P_f}{\delta r} = 0 \tag{4.35}$$

When applying Mohr-Coulomb $P_f = 0$ and introducing a new constant:

$$P = \frac{A_r - A_\theta}{rB_r} = C_0^* \frac{k^* + 1}{H + \lambda} \tag{4.36}$$

Dividing eq. 4.33 with eq. 4.29 gives $C_\theta / B_r = k^{*2}$:

$$\frac{\delta^2 u}{\delta r^2} + \frac{1}{r}\frac{\delta u}{\delta r} - k^{*2}\frac{u}{r^2} = \frac{P}{r} \tag{4.37}$$

Solving eq. 4.37 gives this general solution:

$$u = C_1 r^{k^*} + C_2 r^{-k^*} + \frac{rP}{1 - k^{*2}} \tag{4.38}$$

The radial stress then becomes:

$$\sigma_r = \frac{H^2 - \lambda^2}{H(k^{*2} + 1) - 2\lambda k^*}\left[2k^* C_1 r^{k^* - 1} - \frac{C_0^*}{H^2 - \lambda^2} - \frac{P}{k^* - 1}\right] \tag{4.39}$$

With the boundary conditions saying that at $r = R$ and $\sigma_r = P_w$:

$$P_w = \frac{H^2-\lambda^2}{H(k^{*2}+1)-2\lambda k^*}\left[2k^* C_1 R^{k^*-1} - \frac{C_0^*}{H^2-\lambda^2} - \frac{P}{k^*-1}\right] \tag{4.40}$$

Then solving eq. 4.40 with respect on C_1 with $P_w = 0$ yields:

$$C_1 = C_0^* R^{-k^*-1}\frac{H(k^{*2}+1)-2\lambda k^*}{2k^*(k^*-1)(H^2-\lambda^2)} \tag{4.41}$$

The plastic strain then becomes:

$$d\lambda_p = C_2 r^{-k^*-1} - \frac{C_0^* + C_1 r^{k^*-1}(k^{*2}-1) - \frac{P}{k^*+1}(H-\lambda)}{H(k^{*2}+1)-2\lambda k^*} \tag{4.42}$$

The radial displacement in the elastic zone can be written as:

$$u = \frac{\sigma_h}{H+\lambda} r - \frac{C_2{}'}{H-\lambda}\frac{1}{r} \tag{4.43}$$

and the stresses are:

$$\sigma_r = \sigma_h + \frac{C_2{}'}{r^2} \tag{4.44}$$

$$\sigma_\theta = \sigma_h - \frac{C_2{}'}{r^2} \tag{4.45}$$

As for the stress derivation for Mohr-Coulomb in section 4.1, the boundary between the elastic region and the plastic at $r = R_p$:

$$\sigma_r^{elastic} = \sigma_r^{plastic} \tag{4.46}$$

The Tresca approach in (Fjær et al, Ch. 4, 2008) [7] requires that the plastic strain is zero at $r = R_p$, which makes it only to include plastic strain. In this derivation, both elastic and plastic strain is evaluated. To fulfill this requirement, the boundary condition here, allows no displacement between the elastic and the plastic region, thus:

$$u_{elastic} = u_{plastic} \tag{4.47}$$

Eq. 4.43 equals eq. 4.38 gives:

$$\frac{\sigma_h}{H+\lambda}R_p - \frac{C_2{}'}{H-\lambda}\frac{1}{R_p} = C_1 R_p^{k^*} + C_2 R_p^{-k^*} + \frac{R_p P}{1-k^{*2}} \tag{4.48}$$

The radial stress in the plastic zone is defined as:

$$\sigma_r = \frac{C_0^*}{k^*-1}\Big[\Big(\frac{r}{R}\Big)^{k^*-1} - 1\Big] \tag{4.49}$$

Eq. 4.46 allows putting eq. 4.44 equals eq. 4.49 at the plastic-elastic boundary:

$$\sigma_h + \frac{C_2{}'}{R_p^2} = \frac{C_0^*}{k^*-1}\Big[\Big(\frac{R_p}{R}\Big)^{k^*-1} - 1\Big] \tag{4.50}$$

Which gives:

$$C_2{}' = \Big[\frac{C_0^*}{k^*-1}\Big[\Big(\frac{R_p}{R}\Big)^{k^*-1} - 1\Big] - \sigma_h\Big]R_p^2 \tag{4.51}$$

Combining this with 4.36, 4.41 and 4.49 gives:

$$C_2 = \frac{HR_p^{k^*+1}}{H^2-\lambda^2}\Big[2\Big(\sigma_h + \frac{C_0^*}{k^*-1}\Big) - \frac{C_0^*}{k^*-1}\Big(\frac{R_p}{R}\Big)^{k^*-1}\frac{(k^*+1)^2}{2k^*}\Big] \tag{4.52}$$

Eqs 4.44 and 4.45 at $r = R_p$ require that they have fulfilled the failure criterion:

$$\sigma_1{}' = C_0 + k\sigma_3{}' \tag{4.53}$$

Where k is the initial friction factor $tan^2\beta$. The plastic zone radius is then:

$$\frac{R_p}{R} = \left[1 + \frac{2\sigma_h - C_0}{C_0^*}\frac{k^* - 1}{k + 1}\right]^{\frac{1}{k^*-1}} \tag{4.54}$$

The total strain in the plastic zone is:

$$\begin{aligned} \frac{u}{r} = \frac{2H\sigma_h}{H^2 - \lambda^2}\Big(\frac{R_p}{R}\Big)^{k^*+1} + \frac{C_0^*}{2k^*(k^* - 1)(H^2 - \lambda^2)}\Big[(H(k^{*2} + 1) - 2\lambda k^*)\Big(\frac{r}{R}\Big)^{k^*-1} \\ -2k^*(H - \lambda) - H\Big[\Big(\frac{R_p}{R}\Big)^{k^*-1}(k^* + 1)^2 - 4k^*\Big]\Big(\frac{R_p}{r}\Big)^{k^*+1}\Big] \end{aligned} \tag{4.55}$$

and the stresses:

$$\sigma_r = \frac{C_0^*}{k^* - 1}\Big[\Big(\frac{r}{R}\Big)^{k^*-1} - 1\Big] \tag{4.56}$$

$$\sigma_\theta = C_0^* + k^*\frac{C_0^*}{k^* - 1}\Big[\Big(\frac{r}{R}\Big)^{k^*-1} - 1\Big] \tag{4.57}$$

The strain in the elastic zone is:

$$\frac{u}{r} = \frac{\sigma_h}{H + \lambda} - \frac{1}{H - \lambda}\Big[\frac{C_0^*}{k^* - 1}\Big[\Big(\frac{R_p}{R}\Big)^{k^*-1} - 1\Big] - \sigma_h\Big]\Big(\frac{R_p}{r}\Big)^2 \tag{4.58}$$

and the stresses:

$$\sigma_r = \sigma_h - \Big[\sigma_h - \frac{C_0^*}{k^* - 1}\Big[\Big(\frac{R_p}{R}\Big)^{k^*-1} - 1\Big]\Big]\Big(\frac{R_p}{r}\Big)^2 \tag{4.59}$$

$$\sigma_\theta = \sigma_h + \Big[\sigma_h - \frac{C_0^*}{k^* - 1}\Big[\Big(\frac{R_p}{R}\Big)^{k^*-1} - 1\Big]\Big]\Big(\frac{R_p}{r}\Big)^2 \tag{4.60}$$

Checking for eq. 4.47 and 4.46:

$$\frac{u_{elastic}}{R_p} = \frac{2H\sigma_h}{H+\lambda} - \frac{1}{H-\lambda}\frac{C_0^*}{k^*-1}\left[\left(\frac{R_p}{R}\right)^{k^*-1} - 1\right] = \frac{u_{plastic}}{R_p} \tag{4.61}$$

$$\sigma_r^{elastic} = \frac{C_0^*}{k^*-1}\left[\left(\frac{r}{R}\right)^{k^*-1} - 1\right] = \sigma_r^{plastic} \tag{4.62}$$

Which proves the calculations are correct. Also note that the boundary conditions in eq. 4.45 and 4.47 do not include continuity in tangential plane, just like the Mohr-Coulomb derivation in section 4.1.

4.4 Application of plastic strain deformation

This section is going to review the application of the strain deformation derived in previous section. It will investigate how different parameters affect the deformation around a well. These parameters include the altered plastic parameters as well as the horizontal stress. The calculations will be based on eq. 4.55 and assume the gap is closed between formation and casing. This means that the u/R-ratio has to be approximately 0,25. Figure 4.6 describes the closing process on how the formation moves towards a casing due to plastic strain deformation. With the notation in the figure, the u/R-ratio becomes:

$$u/R = \frac{R - R_{def}}{R} \tag{4.63}$$

Figure 4.6 does not illustrate when the annulus is totally sealed and the corresponding u/R-ratio here is therefore lower.

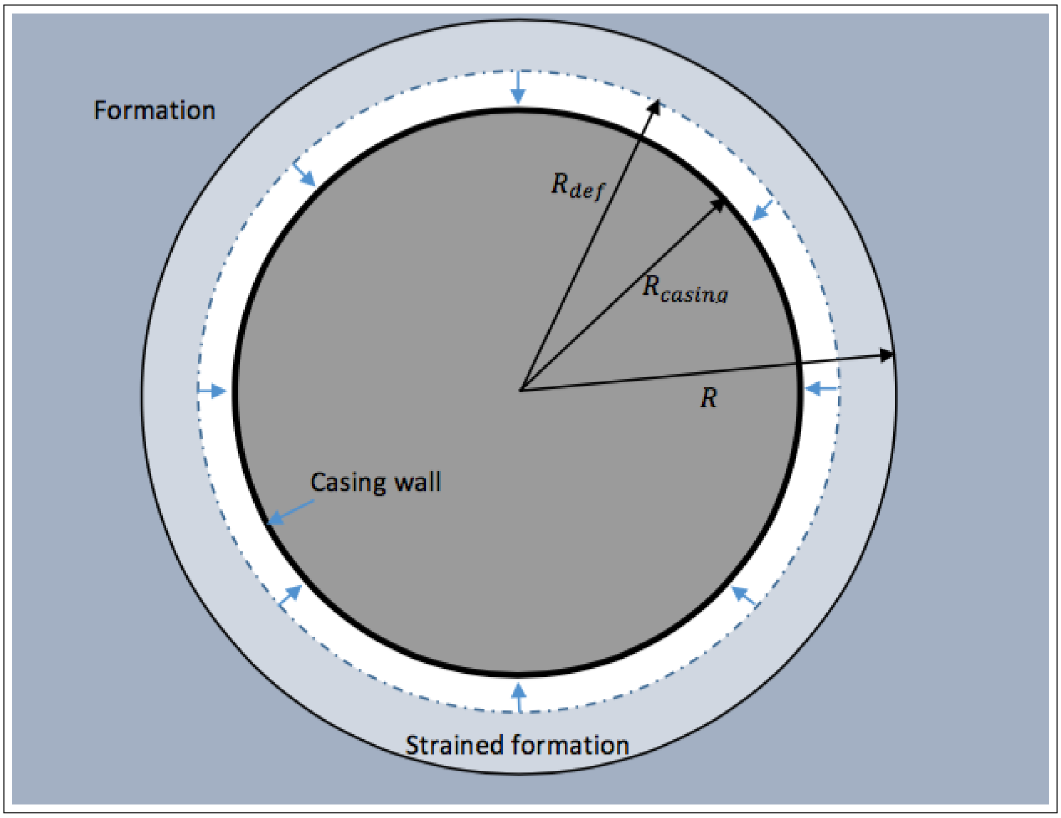

Figure 4.6: A vertical borehole with a formation deforming towards casing.

Determining the horizontal stress

As mentioned previously, eq. 4.55 gives the total strain due to plastic deformation. The horizontal stress in this equation can be used as a parameter to determine how easy a rock can seal around a casing. The lower horizontal stress eq. 4.55 requires to reach a u/R-ratio, the better suited is the rock to deform around a casing. Eq. 4.55 has σ_h and R_p as unknown and the plastic radius eq. 4.54 needs therefore to be included. Now, there are two equations with two unknowns, but the complexity of eq. 4.55 makes the problem too difficult to solve it analytically. It is therefore suggested to solve eq. 4.55 for σ_h and eq. 4.54 for R_p with iteration. This iteration process starts with an initial guess on a σ_h in eq. 4.54. The next step is to insert the new R_p (computed in eq. 4.54) into eq. 4.55 which yields a new σ_h. This σ_h is then inserted back to eq. 4.54. The procedure continues until both σ_h and R_p converges to their true values, and operation can be conducted by a simple while-loop in MATLAB or LOOKUP-function in Excel.

4.5 Evaluation of elastic strain

Eq. 4.55 gives the result as total strain deformation, and does not distinguish whether the main contribution to the deformation comes from plastic strain or elastic strain. Equation 4.43 which (Fjær et al, Ch. 4, 2008) [7] denotes as:

$$u/R = \frac{\sigma_h}{H+\lambda} + \frac{\sigma_h}{H-\lambda} \tag{4.64}$$

This equation excludes pore and well pressure and describes only elastic displacement on the borehole wall. Applying elastic parameters in section 4.6 ($H = 2500$ MPa and $\lambda = 500$ MPa) and corresponding horizontal stress $\sigma_h = 10$ MPa into 4.64 gives an elastic strain on $u/R = 0,0083$. This means that the well radius decreases just below 1 % by only allowing elastic strain.

4.6 Plastic parameter evaluation

This section is going to investigate what impact different plastic parameters i.e. k, k^*, C_0 and C_0^* have on plastic strain deformation around a well. The horizontal stress is used as an interpretation parameter to this purpose. The analysis will be conducted by adjusting the plastic parameters one by one, while the remaining parameters are kept constant. The initial parameters are following:

- $k = 3$.
- $k^* = 2$.
- $C_0 = 10$ MPa.
- $C_0^* = 1$ MPa.
- Borehole radius $R = 0,2225$ m (never changed).
- Uniaxial compaction modulus $H = 2500$ MPa (never changed).
- Lame's parameter $\lambda = 500$ MPa (never changed).
- $u/R = 0,25$ (never changed).

Where H and λ are constants which are assumed.

The analysis on how the horizontal stress becomes affected by change in plastic parameters can be conducted in both MATLAB and Excel. The general methodology involves the procedure conducted when determining the horizontal stress σ_h in previous section. This operation is then repeated separately for each new plastic parameter incrementally. According to Mohr-Coulomb, the general rule for evaluation area is that $k^* \leq k$ and $C_0^* \leq C_0$.

4.6.1 Evaluation of k

Figure 4.7 shows that k (orange) is evaluated from $2 \leq k \leq 3$. The intersections of reference line σ_h (dashed red) and reference line for k^* (dashed black) and k (dashed blue) indicate the initial values. At this state, the formation requires a horizontal stress on 10 MPa in order to reach a plastic strain deformation ratio $u/R = 0,25$. Initially, when $k = k^* = 2$, the required horizontal stress is approximately 9 MPa. When k reaches 3, the required horizontal stress is the same value as in the initial condition (10 MPa). This means that the relative change in horizontal stress is approximately 11 %, while the relative change in friction factor k is 50 %.

4.6.2 Evaluation of k^*

Figure 4.7 shows that k^* (blue) is evaluated in the area from $1,1 \leq k^* \leq 3$. As for the k-evaluation, the intersections of reference line σ_h (dashed red) and reference line for k^* (dashed black) and k (dashed blue) indicate the initial values. Eq. 4.54 restricts k^* not to approach 1 as R_p in that case diverges and a solution will not exist. Initially, at $k^* = 1,1$, the required horizontal stress is approximately 9 MPa, and when k^* increases, figure 4.7 indicates the horizontal stress increases with approximately same rate as it did with k.

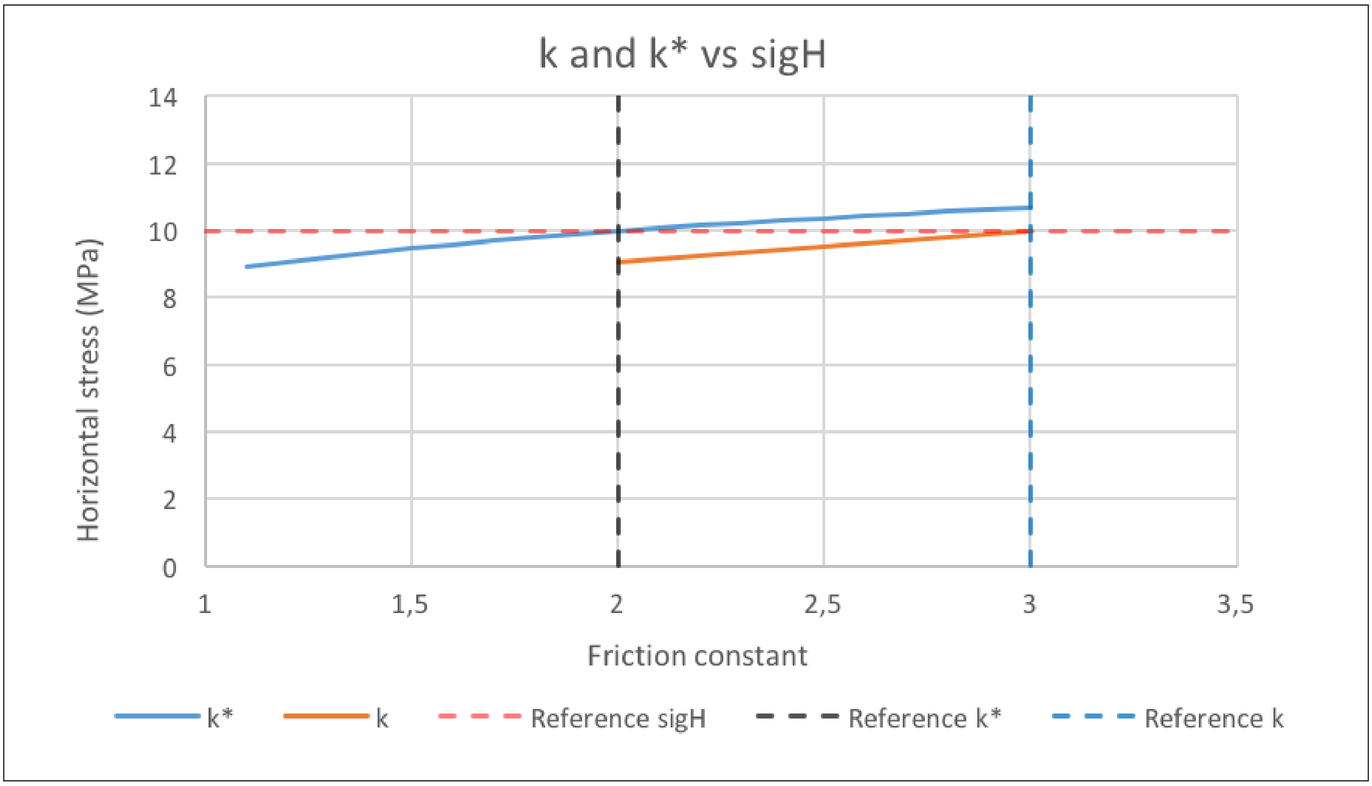

Figure 4.7: Horizontal stress as a function of friction constants

4.6.3 Evaluation of C_0

Figure 4.8 presents evaluation of C_0 in the area from $1 \leq C_0 \leq 19,5$. The intersections of reference line σ_h (dashed red) and reference line for C_0 (dashed black) and C_0^* (dashed blue) indicate the initial values. Initially, when $C_0 = C_0^* = 1$ MPa, the required horizontal stress approximately 7,5 MPa. As the compressive strength C_0 increases, the horizontal stress also increases. At initial condition ($C_0 = 10$ MPa), the horizontal stress is also 10 MPa, and it increases with same rate until it reaches approximately 13,7 MPa. At this state, C_0 has a value of 19,5 MPa which indicates relative increase of 1 850 % from the initial value, while the relative increase in horizontal stress is approximately 83 %.

4.6.4 Evaluation of C_0^*

Figure 4.7 shows that C_0^* (blue) is evaluated in the area from $1 \leq C_0^* \leq 10$. As for the C_0-evaluation, the intersections of reference line σ_h (dashed red) and reference line for C_0 (dashed black) and C_0^* (dashed blue) indicate the initial values. As C_0^* increases from 1 MPa to 10 MPa, the horizontal stress increases from 10 MPa to almost 36,5 MPa. This indicates a relative increase for σ_h to be 265 % and a relative change in C_0^* is 900 %.

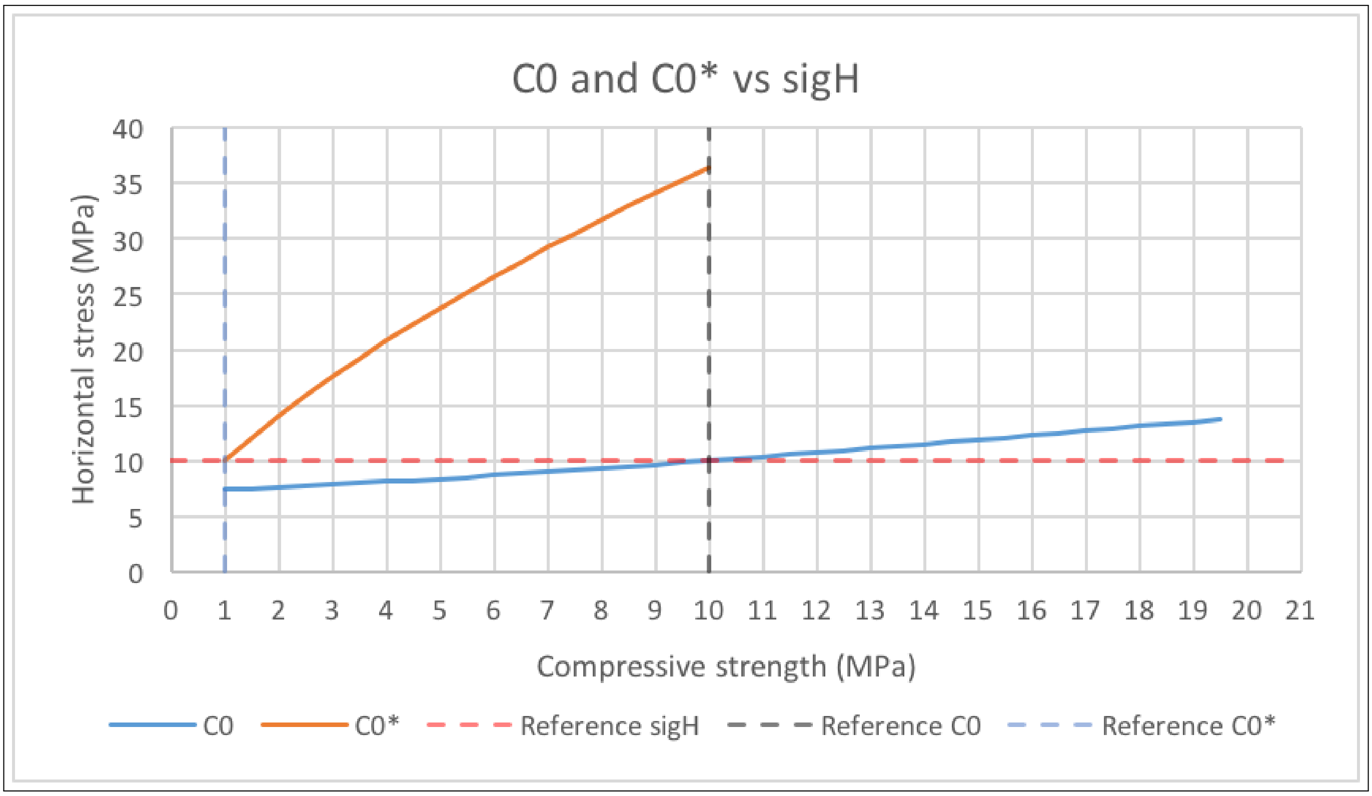

Figure 4.8: Horizontal stress as a function of compressive strength of rock.

4.7 Analytical results of stress distribution around a borehole

This section will investigate stress distribution around a borehole for both constant and altered plastic parameters based on derivation conducted in section 4.1. The horizontal stress in section 4.6 is calculated to be 10 MPa with initial parameters. It is therefore decided to investigate the stress distribution around a borehole with $\sigma_h = 10$ MPa for both constant and altered parameters. Hence, the analysis for altered parameters will represent the stress distribution when the deformation has closed 25 % of the well radius.

4.7.1 Stress distribution for constant plastic parameters

Figure 4.9 shows the stress distribution for the data presented below the figure. At the borehole wall the radial stress $\sigma_r = P_w = 0$ and it increases linearly until approximately $r/R = 1,5$ where the radial stress slope starts to decrease as it approaches the far field horizontal stress $\sigma_h = 10$ MPa. The tangential stress is $\sigma_\theta = 10$ MPa at the borehole wall and increases up to 17,5 MPa at the boundary between plastic and elastic region $R_p/R = 1,2$. Further, the tangential stress decreases as it approaches the far field horizontal stress $\sigma_h = 10$ MPa.

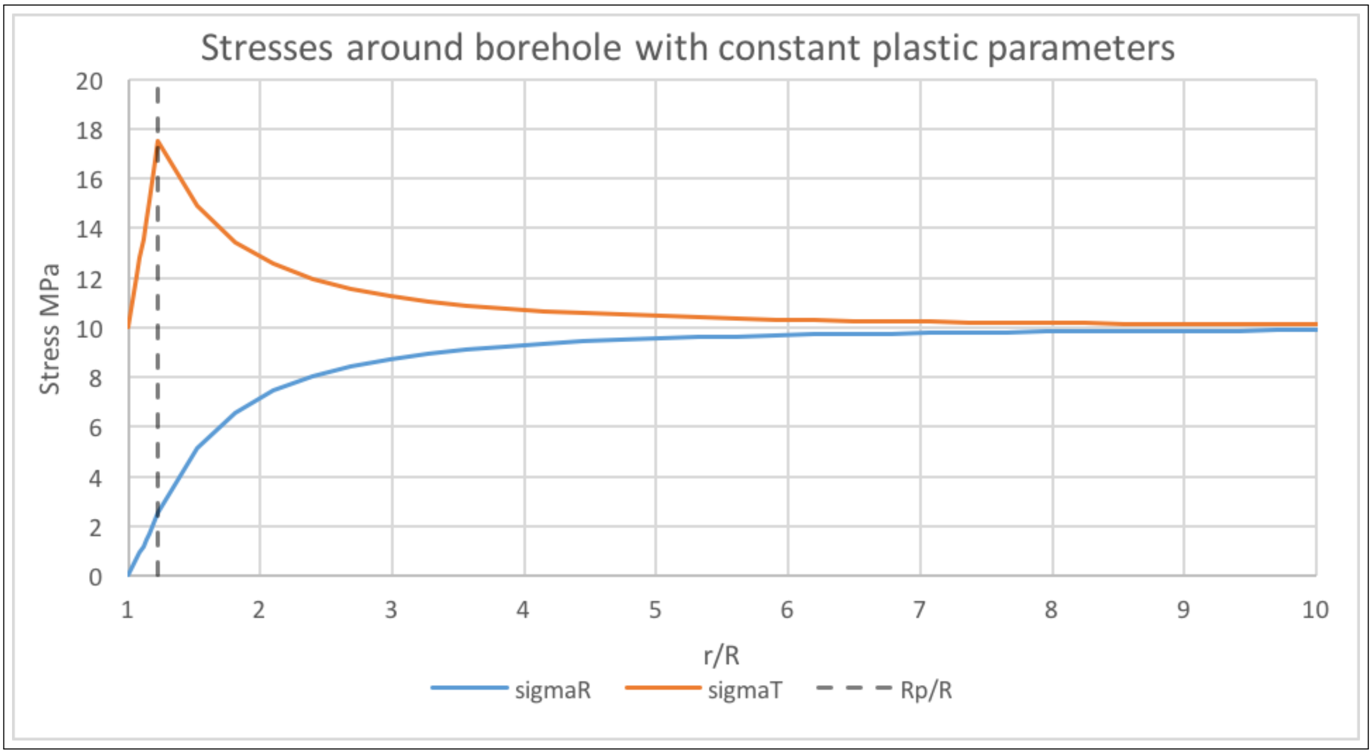

Figure 4.9: Stresses around a borehole with constant plastic parameters

Data for figure 4.9

- Isotropic horizontal far field stress $\sigma_h = 10$ MPa.
- $C_0 = C_0^* = 10$ MPa.
- $k = k^* = 3$.
- Borehole radius $R = 0,2225$ m.
- Well pressure $P_w = 0$ MPa.
- Pore pressure $P_f = 0$ MPa.

4.7.2 Stress distribution for altered plastic parameters

Figure 4.10 shows the stress distribution for the data presented below the figure. At the borehole wall the radial stress $\sigma_r = P_w = 0$ and it increases linearly until the boundary between plastic and elastic region $R_p/R = 3,5$. At this point, the radial stress suddenly changes over to elastic behaviour and the stress increase slows down as it approaches the horizontal far field stress $\sigma_h = 10$ MPa. The tangential stress is $\sigma_\theta = 1$ MPa at the borehole wall and increases up to 6 MPa at the edge of the plastic region $R_p/R = 3,5$. At the transition from plastic to elastic region, the tangential stress shows discontinuity as it suddenly bounces up to 17,5 MPa. Further, the tangential stress decreases as it approaches the far field horizontal stress $\sigma_h = 10$ MPa.

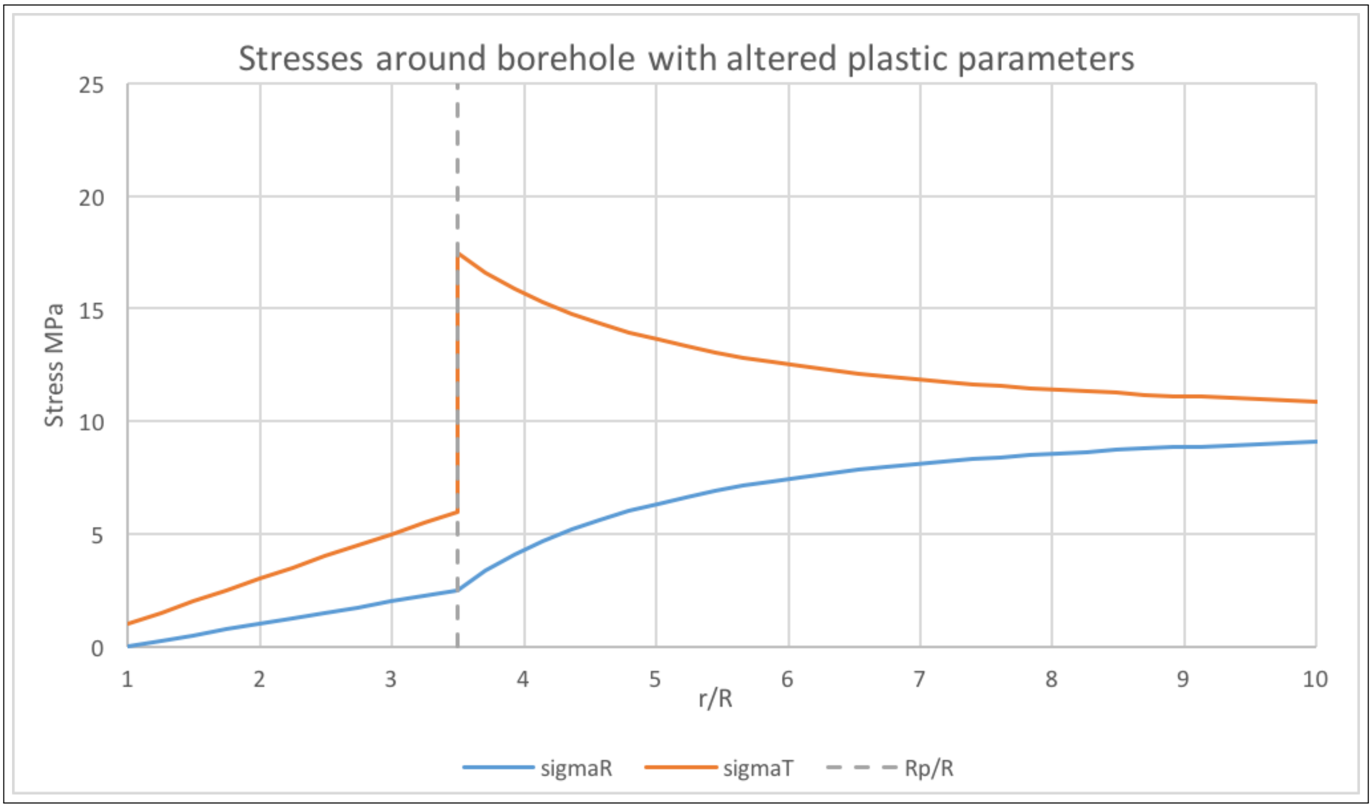

Figure 4.10: Stresses around a borehole with altered plastic parameters

Data for figure 4.10

- Isotropic horizontal far field stress $\sigma_h = 10$ MPa
- $C_0 = 10$ MPa
- $C_0^* = 1$ MPa
- $k = 3$
- $k^* = 2$
- Borehole radius $R = 0,2225$ m
- Well pressure $P_w = 0$ MPa
- Pore pressure $P_f = 0$ MPa

5 Discussion

5.1 Sources of error in the simulations

Through the simulations of both calibration and creep around a well, different sources of error are discovered. These involve limitations of code and the mimicking, as well as doubtful assumptions regarding downhole conditions in the borehole simulation.

- **Horizontal stress**
  The model requires an effective horizontal stress $\sigma_h = 30$ MPa to make the rock creep. This is high horizontal stress comparing to the TVD on 1000 m. (Zoback et al, 2003) [17] suggests an effective horizontal stress on $\sigma'_h = 0,6\sigma'_z$, which at TVD on 1000 m approximately gives an effective horizontal stress $\sigma_h = 6$ MPa. The requirement for high horizontal stress to make the model creep, proves that Haynesville is not well suited for the purpose as a well barrier. Haynesville is therefore chosen as a reference due to its easy accessible creep data rather than its well barrier applicability.

- **Simplicity of model**

  The simulation simulates in 2D, and therefore only includes stresses to act in the x-y plane. For the borehole simulation, the vertical stress is excluded and creep drive mechanism is controlled by applied horizontal stress, while in reality, vertical stress is an important parameter regarding creep around a wellbore. This proves that the code does not fully simulate the correct creep mechanism. Another problem regarding this 2D code, is that it has a rather simplified yield criterion (Described in section 2.1). (Li et al, 2014) [18] developed a model for PFC3D which among other failure criteria, included the Mohr-Coulomb. Such criteria are not yet developed for 2D.

  The grains which are simulated in this thesis are shaped as balls, while in reality, the grains in a shale has a rather flaky shape. In order to mimic a shale more thoroughly, flaky ball structures can be implemented. This may change the strain and creep results.

- **Calibration error**
  There are uncertainties related to the calibration of parameters such as threshold stresses, bond strength and creep rate. For instance, the calibration test detects little change in strain rate by changing threshold stresses. This is due to the high differential stress P_{diff} applied in this test. For simulations where lower differential pressure is applied, change in threshold stresses might have larger impact on creep.
- **uRate**
  The uRate may affect the initial conditions at the borehole wall. Too high uRate can for instance result in dynamic effects and break outs, and too low may result in no annulus development. The dynamic effects and break outs affect the size of the initial gap and the stress distribution around the well. Unsuitable uRate, as a source of error, should therefore be considered if unexpected initial gap and stress distribution results occur.
- **Inaccuracy**
  Output plotting and printing parameters from PFC can be inaccurate. Figure 5.1 illustrates an example of this inaccuracy; It shows the location of where the numerical analysis on stress distribution around wellbore is conducted. The radial and tangential stress is calculated and recorded in each circle separately. This means that the evaluation of stresses around a borehole only represent a small part of the model, and not the stress distribution around the whole well. Figure 5.1 also indicates that the area closest to the borehole wall is not evaluated. It is therefore not possible to determine the exact stress condition at the wellbore wall.

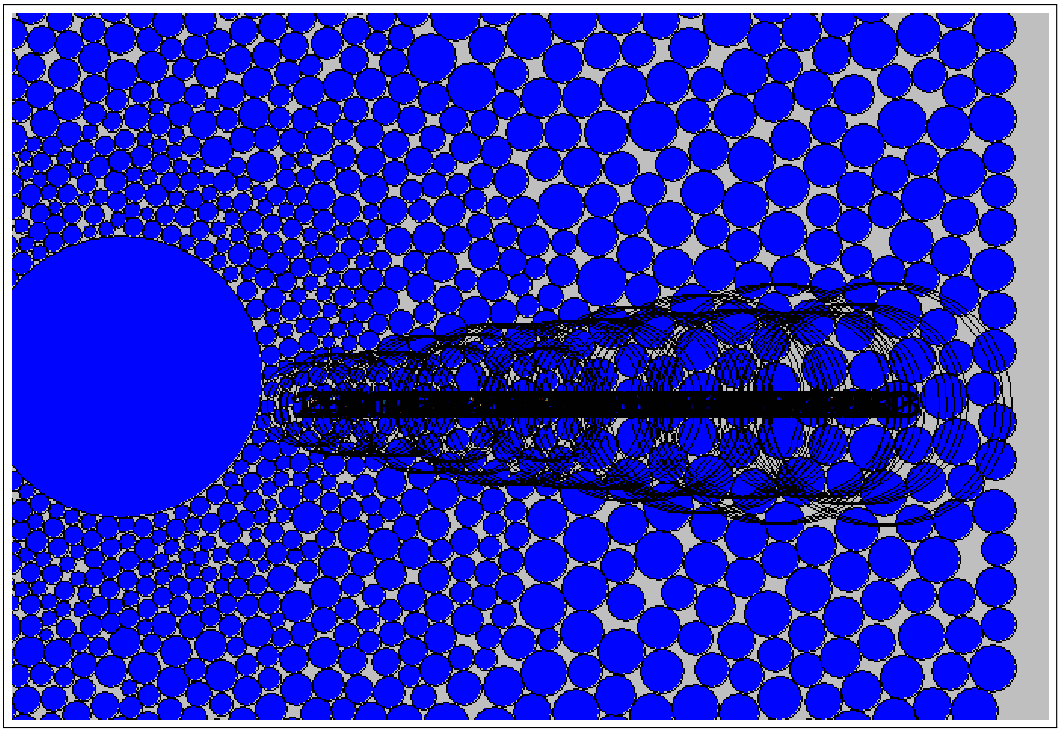

Figure 5.1: A ball plot of a fully closed annulus. The black circles illustrate the location of stress distribution analysis.

5.2 Discussion of simulation results

The numerical analyses involve simulations on calibration test and creep around a borehole. The calibration test mimics the strain rate on a biaxial test to the strain rate for a triaxial creep test on a real shale core specimen (Haynesville). The strain rate is mimicked by adjusting the bond strength between elements and creep rate. To achieve the strain rate recorded in figure 3.2 $strainRate = 1,5 * 10^{-8}s^{-1}$, the bond strength and creep rate are required to be 30 MPa and 0,000033 respectively. The recorded data from the calibration test are then applied in the well scale simulation in order to mimic creep around a borehole for Hayneseville.

The creep threshold for the calibration test is initially decided to be 1 MPa for both the shear and tensile threshold. Section 3.1.3 evaluates the strain rate for the calibration test with no creep threshold. Figure 3.7 shows no significant difference between the strain rates for the different threshold stresses. This proves that creep threshold is not capable to affect the strain rates when large differential stress P_{diff} is applied. It is therefore decided to investigate how the creep threshold affects closure around a borehole where the model's differential stress between x-y directions is zero.

Figure 3.19 presents the relative gap and relative pressure on casing vs time when the creep tensile and shear threshold are both increased to 1 MPa. After 277 days, the gap is reduced to 50 % of its initial size, and at t=1076 days, the gap is reduced to 10 % of its initial size. One should note that the initial gap in this case is related to the requested initial gap in the code. The fact that the gap at t=0 days is 80 % indicates that there has been some deformation prior to the creep initiation, which might be a result of too high uRate. Figure 3.8 also indicates small break outs at the borehole wall which according to the previous section backs up this argument. After 1076 days the relative average pressure on casing has reached 15 % of the applied horizontal stress (0,15*30 MPa = 4,5 MPa). Pressure on casing gives an indication on how the formation bonds with casing, but it does not describe the quality of the barrier. This is because the parameter is unable to detect the sealing capabilities of the formation, which can for instance be destroyed by crack development and break outs. Visual interpretation of figure 3.13 at t=1076 shows that there are still gaps and spaces fluid easily can penetrate. Figure 3.14 also concludes that the rock in this simulation has not reached a sufficient barrier as there is still 10 % gap left to seal.

Figure 3.14 presents the relative gap and relative pressure on casing vs time when the creep threshold is absent. After 360 days, the gap has reduced to approximately 30 % of its initial size, and at t=1069 days, the gap is reduced to under 5 % of its initial size. The relative average pressure on casing is 0,4* 30 MPa = 12 MPa at this stage. Unlike the simulation in section 3.2.2, the initial gap prior to creep initiation is here 100 %. This contradicts the argument on high uRate as both simulations use the same uRate (figure 3.9). The reason for the break outs and initial deformation in section 3.2.2 remains therefore unknown. When it comes to the gap development around wellbore in section 3.2.3, figure 3.19 shows that the relative gap remains stable (just below 5 %) the last 100 days of the simulation. During the same period, the relative average pressure on casing increases. This is also an indication that the relative pressure parameter is invalid when determining the sealing capabilities of a formation pushing on casing.

When comparing the results from creep deformation around wellbore in section 3.2.2 and section 3.2.3, it is clear that the simulation without creep threshold experiences significantly more deformation compare to the simulation which included these parameters. Adding the fact that the calibration test is not able to detect any considerable difference in the strain rates while changing these threshold stresses, induces huge uncertainties regarding this parameter. In order to reduce the uncertainties on the creep threshold for future work, it is suggested to mimic a softer shale. A softer shale requires less differential stress in order to initiate creep. The applied differential stress in the calibration simulation has to correspond to the differential stress of the real rock specimen. Due to this reduction in differential stress, the true threshold stress may be easier determined.

The different graphs in figure 3.15 and figure 3.20 present how the stress distribution develops during creep around a well for approximately 1000 days. The behaviours of tangential stresses indicate that the model undergoes plasticity near wellbore. This is because they tend to have a relatively steep slope before the peak, and the region before this peak, is often referred to as plastic region. Despite different threshold conditions, both analyses indicate more or less the same behaviour for all time step evaluated. As mentioned in section 5.1, the analyses on stresses around wellbore may give some errors regarding inaccuracy, and the spiky and irregular behaviour of the various stresses might be a result of that.

5.3 Sources of error in evaluation on elastic and plastic strain deformation

This section lists up and elaborates assumptions and corresponding errors to the total strain deformation model.

- **Ideal elastic and plastic behaviour**
  The total strain deformation model assumes ideal elastic and plastic behaviour. This means that a rock will act like figure 4.1 or figure 4.3 with increasing load. In reality, a rock may start softening/hardening when it exceeds its failure strength (Brady et al, 1973) [14]. The beyond elasticity behaviour will then either be decreasing (softening) or increasing (hardening) as a function of strain. The total strain deformation model excludes possibility for these behaviours.

- **No pore pressure**
  The total strain deformation model assumes no pore pressure. This is an assumption due to Mohr-Coulomb criterion as it requires complete drainage.

- **No well pressure**
  The total strain deformation model assumes no well pressure. Allowing well pressure requires non-permeable borehole wall as the the model does not include pore pressure.

- **Sealing capabilities**
  The total strain deformation model does not evaluate the rock's capabilities to establish a sufficient barrier according to the requirement of authorities. Although a borehole wall has reached sufficient deformation, cracks or break outs may have been developed and destroyed the rock's sealing capabilities.

5.4 Discussion of plastic and elastic deformation results

Section 4.6 and section 4.5 conduct analyses on how different parameters influence the abilities of a rock to deform around a borehole. These are now going to be discussed, and the discussion starts with whether this total strain deformation (eq. 4.55) is mainly a result of plastic strain or elastic strain: The total strain deformation allows 25 % closure of the well radius with the initial given rock properties and corresponding stress condition applied in section 4.6. With the same rock properties and stress condition, the elastic strain evaluation in section 4.5 shows that the wellbore closes below 1 % by only allowing elasticity. This indicates that the elasticity contributes very little to the total strain deformation compared to the plastic strain. Thus, elastic parameters such as H and λ are not essential parameters regarding total strain deformation around a borehole.

The elastic strain analysis in section 4.5 concludes that by only allowing elastic strain, there would only be under 1 % deformation of wellbore. As this indicates that the elastic contribution to the deformation is very little, it is decided to conduct analysis on plastic parameters, k, k^*, C_0 and C_0^*. These analyses investigate what impact each of these parameters have on a rock's ability to deform around a well. The discussion will focus on the results from figure 4.7 and figure 4.8.

Figure 4.7 presents graphs of both k and k^* and shows that the required horizontal stress to reach $u/R = 0,25$, varies with 1 MPa when changing k and 2 MPa when changing k^*. It is important to note k^* is evaluated two times the range of k. This indicates that they have equal slope and therefore equal impact on the ability of a rock to deform.

Figure 4.8 presents the horizontal stress σ_h as a function of C_0 and C_0^*. By maintaining C_0^* as constant, the horizontal stress required to reach 25 % closure varies from $\sigma_h = 8$ MPa to $\sigma_h = 14$ MPa when evaluating $1 < C_0 < 19,5$ MPa. By maintaining C_0 as constant, the horizontal stress required to reach 25 % closure varies from $\sigma_h = 10$ MPa to $\sigma_h = 36,5$ MPa when evaluating $1 < C_0^* < 10$ MPa.

The slope indicates change in horizontal stress per incremented variable, and the magnitude in slope therefore describes the impact each variable has on the ability of a rock to deform. Analyses in section 4.6 show that the unconfined residual strength C_0^* has a significant steeper slope than k, k^* and C_0. This indicates that the unconfined residual strength C_0^* is an important parameter compared to the other plastic parameters regarding a rock's ability to deform around a well.

Figure 4.9 presents the stress distribution around a borehole according to Mohr-Coulomb failure criterion (section 4.1). The figure describes when failure occur with constant plastic parameters ($C_0 = C_0^*$ and $k = k^*$). These parameters also decide the size of the plastic zone. Figure 4.10 presents the stress distribution around wellbore when altered plastic parameters are introduced and the well has undergone a deformation of 25 %. Unlike figure 4.9 the tangential stress shows discontinuity in the transition between plastic and elastic zone. This is not a surprising result as Mohr-Coulomb criterion only requires continuity in the radial stress (eq 4.11 and eq 4.46). Except for the discontinuity, figure 4.10 also shows that the plastic zone is significant greater when allowing altered plastic parameters.

6 Conclusion

This thesis has conducted creep simulations in PFC and derived an analytical expression on plastic and elastic strain deformation around a borehole according to the Mohr-Coulomb criterion. The creep simulation investigated the impact of change in threshold stresses, while the analytical part examined the importance for various parameters for a rock's ability to strain deform around a well. Following conclusions are obtained from this work:

- The PFC simulations on creep around a borehole discovered major differences in a rock's ability to close the gap between formation and casing when changing creep threshold stresses.
- The calibration tests which mimicked strain rates from a real rock specimen into PFC were unable to detect any significant difference in strain rate when changing the creep threshold stress τ_0. This leads to huge uncertainties regarding calibration of this parameter. The absence of change in strain rate is due to high differential stress P_{diff} in the simulation.
- It is possible to reduce these uncertainties by mimicking from a softer rock specimen than Haynesville. Softer rock requires lower differential stress P_{diff} to induce creep. This allows the corresponding differential stress in the simulation also to be reduced.
- Evaluation of elastic deformation indicates that elastic strain contributes little to the total strain deformation around a borehole.
- Analyses on total strain deformation around a borehole show that the unconfined residual strength C_0^* has large impact on the rock's ability to close the annulus between casing and formation.
- Plasticity may explain closure around a wellbore, but it is important to note that these analytical strain analyses do not evaluate the sealing capabilities of a rock.

References

[1] Stephen Williams, Truls Carlsen, Kevin Constable, and Arne Guldahl. Identification and qualification of shale annular barriers using wireline logs during plug and abandonment operations. *SPE/IADC*, (119321), 2009.

[2] Earl W. McDaniel. Cement technology for borehole plugging: An interim report permeability measurements cementitious solids. Master's thesis, Oak ridge national laboratory, 1980.

[3] M. Torsæter, J. Todorovic, J.F. Stenebråten, E. Fjær, and G.K. Gabrielsen. Shale smearing at the borehole wall during drilling. *ARMA*, 14(7401), 2014.

[4] Jon Steinar Folstad. Shale as a permanent barrier after well abandonment. Confidential, NTNU, 2015.

[5] Øyvind Skomedal. Stress distribution around borehole during creep and casing expansion. 2015.

[6] E Fjær, I Larsen, R.M Holt, and A Bauer. A creepy model for creep. *ARMA*, 14(7398), 2014.

[7] Erling Fjær, Rune M. Holt, Per Horsrud, Arne M. Raaen, and Rasmus Risnes. *Petroleum Related Rock Mechanics*. Elsevier, 2nd edition, 2008.

[8] J. C. Jaeger, N. G. W. Cook, and R. W Zimmermann. *Fundamentals of Rock Mechanics*. Balckwell Publishing, 4th edition, 2007.

[9] Hiroki Sone and Mark D. Zoback. Time-dependent deformation of shale gas reservoir rocks and its long-term effect on the in situ state of stress. *International Journal of Rock Mechanics & Mining Sciences*, 69:120–132, 2014.

[10] A. Bauer, R.M. Holt, J. Stenebråten, E.F. Sønstebø, and L. Marøen. Thermally induced compaction of shales. *ARMA*, 14(7504), 2014.

[11] Chun-Liang Zhang, Tilmann Rothfuchs, Kun Su, and Nasser Hoteit. Experimental study of the thermo-hydro-mechanical behaviour of indurated clays. *Physics and Chemistry of the Earth*, 32:957–965, 2006.

[12] Matthew R. Kuhn and James K. Mitchell. New perspevtive on soil creep. *Journal of Geotechnical Engineering*, 3(119):507–524, 1993.

[13] E Fjær, J.S Folstad, and L Li. How creeping shale may form a sealing barrier around a well. *ARMA*, 16(482), 2016.

[14] B. T. Brady, W. I. Duvall, and F. G. Horino. An experimental determination of the true uniaxial stress-strain behavior of brittle rock. *Rock mechanics*, 5(2):107–120, 1973.

[15] Hiroki Sone and Mark D. Zoback. Mechanical properties of shale-gas reservoir rocks — part 2: Ductile creep, brittle strength, and their relation to the elastic modulus. *GEOPHYSICS*, 78(5), 2013.

[16] Rasmus Risnes, Rolf K. Bratli, and Per Horsrud. Sand stresses around a wellbore. *Society of Petroleum Engineers Journal*, pages 883–898, December 1982.

[17] M.D. Zoback, C.A. Barton, M. Brudy, D.A. Castillo, T. Finkbeiner, B.R. Grollimund, D.B. Moos, P. Peska, C.D. Ward, and D.J. Wiprut. Determination of stress orientation and magnitude in deep wells. *International Journal of Rock Mechanics & Mining Sciences*, 40:1049–1076, 2003.

[18] Liming Li, Idar Larsen, and Rune M. Holt. Laboratory observation and micromechanics-based modelling of sandstone on different scales. *Rock Mechanincs and Rock Engineering*, DOI 10.1007/s00603-014-0642-5, 2014.